

# Integrated stratigraphy of the Smirra Core (Umbria-Marche Basin, Apennines, Italy): A new early Paleogene reference section and implications for the geologic time scale

Antonio Turtù<sup>a,b,\*</sup>, Vittoria Lauretano<sup>a,2</sup>, Rita Catanzariti<sup>c</sup>, Frits J. Hilgen<sup>a</sup>, Simone Galeotti<sup>d</sup>, Luca Lanci<sup>b,e</sup>, Matteo Moretti<sup>d,f</sup>, Lucas J. Lourens<sup>a</sup>

<sup>a</sup> Department of Earth Sciences, Utrecht University, Heidelberglaan 2, 3584 CS Utrecht, The Netherlands

<sup>b</sup> Alpine Laboratory of Paleomagnetism (ALP), Via Madonna dei Boschi 76, 12016 Peveragno, CN, Italy

<sup>c</sup> Istituto di Geoscienze e Georisorse, CNR, Via G. Moruzzi 1, 56124 Pisa, Italy

<sup>d</sup> Dipartimento di Scienze della Terra, della Vita e dell'Ambiente, University of Urbino, Campus Scientifico "E. Mattei", Via Cà le Suore 2/4, 61029 Urbino, Italy

<sup>e</sup> Department of Pure and Applied Science, University of Urbino, Piazza della Repubblica 13, 61029 Urbino, Italy

<sup>f</sup> Dipartimento di Geoscienze, University of Padova, Via G. Gradenigo 6, 35131 Padova, Italy

## ARTICLE INFO

### Keywords:

Paleocene-Eocene  
Magnetostратigraphy  
Calcareous nannofossil biostratigraphy  
Cyclostratigraphy  
Chronology  
Time scale

## ABSTRACT

Pelagic sections of the Umbria-Marche Basin, in the Northern Apennines (Italy), have provided key geological archives for studying critical intervals of early Paleogene time. In addition to classical sections, the Smirra Coring project provides a new record of relatively undisturbed sediments (~120 m from 4 overlapping holes) of the upper Scaglia Formation (Paleocene – middle Eocene). Here we present a new high-resolution integrated magneto-bio-stratigraphy of the ~93-m composite section drilled in Smirra Holes 1 and 2. The correlation of the magnetostratigraphy to published geomagnetic polarity timescales (GPTSs; CK95, GPTS2004, GPTS2012), as constrained by calcareous nannofossil biostratigraphy, reveals that the cores range from Chron C26r to C21n (Thanetian – Lutetian; ~60 to ~46 Ma). Sedimentation rates range from ~0.6 to ~1 cm/kyr and are comparable with those from coeval sections in the Umbria-Marche Basin. They point to significant discrepancies between existing time scales, which mainly involve the duration of Chron C23 and subchrons within C23n and C24n. Application of the average spectral misfit method on the magnetic susceptibility record reveals a strong signature of orbital forcing and allows an independent estimate of the sedimentation rates. This analysis offers additional insights into solving time scale issues, which mainly concern the duration of Chron C23n. Our results imply a significantly longer duration for C23n.2n, which would accommodate the presence of an extra third 405-kyr eccentricity related cycle in C23n. The Smirra record thus provides new constraints on the early Paleogene time scale, a key record for further cyclostratigraphic and astrochronological research, and a reference framework for paleo-climatic and -oceanographic studies.

## 1. Introduction

The early Paleogene represents a critical time interval in Earth's history as it was characterized by prolonged greenhouse conditions, punctuated by a series of extreme global warming “hyperthermal” events, and culminating in a sustained period of high temperatures known as the Early Eocene Climatic Optimum (EECO; Zachos et al., 2005, 2008; Lourens et al., 2005; Nicolo et al., 2007; Littler et al., 2014; Kirtland Turner et al., 2014; Lauretano et al., 2015). However, large uncertainties still exist in the Geomagnetic Polarity Time Scale (GPTS)

2012 for this time period (Vandenbergh et al., 2012 and reference therein; Westerhold et al., 2015; Lauretano et al., 2016), preventing full understanding of the processes leading to such extreme climatic events. For this reason, it is crucial to generate robust chronostratigraphic frameworks that are based on high-resolution and high-quality magneto-bio-cyclostratigraphic records of continuous sedimentary successions.

The Paleogene Tethyan marine records from the Umbria-Marche (Northern Apennines, Italy) and Belluno (Southern Alps, Italy) basins are suitable for integrated stratigraphic studies that have served as a

\* Corresponding author at: Department of Earth and Life Sciences, Vrije Universiteit, De Boelelaan 1085, 1081 HV Amsterdam, The Netherlands.

E-mail address: [a.turtu@vu.nl](mailto:a.turtu@vu.nl) (A. Turtù).

<sup>1</sup> Department of Earth and Life Sciences, Vrije Universiteit, De Boelelaan 1085, 1081 HV Amsterdam, The Netherlands.

<sup>2</sup> School of Chemistry, University of Bristol, Cantock's Close, BS8 1TS, Bristol, United Kingdom.

basis for insightful environmental reconstructions of this critical time interval. These basins host several stratigraphic reference sections, such as Bottaccione (e.g. Lowrie et al., 1982; Galeotti et al., 2015), Contessa (Jovane et al., 2007; Giusberti et al., 2009; Galeotti et al., 2000), Posagno (Agnini et al., 2006), Cicogna (Dallanave et al., 2009), Alano (Agnini et al., 2011) and Ardo (Dallanave et al., 2012). At present, these sections have provided important paleomagnetic and biostratigraphic archives, allowing global correlations with coeval deep-sea records recovered by the Ocean Drilling Program (ODP) (e.g. Ogg and Bardot, 2001; Parès and Lanci, 2004; Florindo and Roberts, 2005; Bowles, 2006; Suganuma and Ogg, 2006; Edgar et al., 2010) and land-based sections from the southern hemisphere (Dallanave et al., 2015, 2016). These records are generally characterized by high-quality and high-resolution paleomagnetic data, but they often cover only a limited temporal range and/or reveal critical gaps in the magnetostratigraphy. Therefore, new, high-resolution, magneto-bio-stratigraphic records from continuous successions remain critical for providing detailed chronological constraints for the study of the early Paleogene time scale and climatic evolution.

In the Tethyan realm, the Smirra section, outcropping in the northern Apennines of Italy, contains an undisturbed lower to middle Eocene pelagic succession (Franceschi et al., 2015). This site was selected as drilling location and provided a continuous ~120-m long record for the lower Paleogene, retrieved from 4 overlapping holes. Here we present the magnetostratigraphy and quantitative calcareous nannofossil biostratigraphy of the ~93-m composite section drilled in Smirra Holes 1 and 2, spanning the early Paleocene to early-middle Eocene time interval. The results are compared with magnetobiostratigraphic records from coeval land-based sections to test the reliability of the magnetic polarity sequence at Smirra. We computed sedimentation rates for the sedimentary succession and ages for nannofossil bioevents by correlating the magneto-bio-stratigraphy to the GPTSs of Cande and Kent (1995, CK95), Gradstein et al. (2004, GPTS2004) and Gradstein et al. (2012, GPTS2012). The variability in sedimentation rates observed in specific time intervals highlights existing discrepancies between the different GPTSs.

In addition, the Paleogene succession of the Umbria-Marche domain is characterized by a distinct lithological cyclicity, which has previously been investigated in cyclostratigraphic studies (e.g. Galeotti et al., 2010, 2015). Here, we use statistical analysis of the magnetic susceptibility (MS) record acquired by high-resolution scanning of the Smirra cores to verify the presence of orbital forcing. This provides the opportunity to (1) quantify the stratigraphic expression of astronomically induced signals, (2) estimate the optimal sedimentation rate (independently from GPTS correlation) by applying the Average Spectral Misfit method (Meyers and Sageman, 2007; Meyers et al., 2012), (3) evaluate possible implications for future improvements of the GPTS and (4) explore the potential for further detailed cyclostratigraphic studies. Hence, the Smirra coring provides a continuous and integrated magneto- and bio- stratigraphic record across the early Paleocene to early-middle Eocene and holds, therefore, the potential as a new reference chronostratigraphic framework to contribute in resolving existing discrepancies in the Paleocene-Eocene GPTSs.

## 2. Geological setting

The Apennines is a fold-and-thrust belt that developed since the late Oligocene as a result of the convergence between the African and European plates. The pre- and syn-orogenic succession is represented in its northern sector by the pelagic succession of the Umbria-Marche domain (Fig. 1A), deposited since the Late Triassic in the subsiding northern sector of the Adriatic Promontory (D'Argenio, 1970; Channell et al., 1979; Ciarapica and Passeri, 2002). The lower Paleogene succession is represented by the Scaglia Rossa (Turonian pro parte (p.p.) to middle Eocene p.p.) and Scaglia Variegata (middle to upper Eocene) Formations. The Scaglia Rossa Fm. is divided in two Cretaceous (R1 and

R2) and two Paleogene (R3 and R4) members (Alvarez and Montanari, 1988). The R3 and R4 members, with a mean total thickness of 90 m, consist of pink to red limestones and marls, with cherts characterizing the lower Eocene interval (i.e. member R4, middle Ypresian - lower Lutetian). The overlying Scaglia Variegata Fm. is composed of whitish to reddish marly limestones and marls. This formation shows a significant increase in the siliciclastic fraction (~20–30%), reflecting the starting phase of the Alpine-Himalayan orogenesis (Franceschi et al., 2015). All these sediments were deposited at middle to lower bathyal depths (~1500 m; Galeotti et al., 2004; Jovane et al., 2007; Giusberti et al., 2009; Coccioni et al., 2010) and at ~35°N paleolatitude (Muttoni and Kent, 2007).

## 3. Material and methods

### 3.1. Drilling summary

In this work, we study the succession drilled in a disused quarry close to the village of Smirra (43°35'09.40"N 12°40'37.30"E), NE of Cagliari (PU), Italy. The succession has been recovered by drilling 4 holes at different topographic heights in the Smirra quarry in November and December 2013 (Fig. 1B). The bedding in the outcrop, estimated through geological map data (Carta Geologica Regionale - Regione Marche) has a strike of N105°E and an average dip of 15°SSW. The recovered cores cover the uppermost Scaglia Rossa (R4 Mbr., Ypresian p.p.) and basal Scaglia Variegata Fms. (Lutetian p.p.) exposed in the quarry (Franceschi et al., 2015), and then penetrate the whole lower Paleogene Scaglia Rossa Fm., recovering a total of ~120 m of sediments. The drilling was carried out by rotary coring, obtaining cores with an average length of 140 cm that were contained in plastic liners of 10-cm diameter. Hole 1 (hereinafter referred to as Smirra 1) was drilled from the top of the exposed outcrop of the quarry and recovered 41 m of sediments in 30 cores (Fig. 1B, C). Hole 2 (hereinafter referred to as Smirra 2) was drilled from the base of the quarry (Fig. 1B, C). It resulted in the recovery of a total of 43 cores with a total length of ~64 m, and an overlap of ~12 m with Smirra 1. Hole 3 and Hole 4, not included in this study, recovered 9 and 8 cores, respectively, from the lower Paleocene to Upper Cretaceous. The record recovered at Smirra provides a remarkably well-preserved and relatively undisturbed succession of the lower Paleogene pelagic sediments in this area of the Umbria-Marche basin, which otherwise is often strongly tectonized.

### 3.2. Downhole logging and core preparation

Downhole optical logs were acquired using an optical Televue (OPTV), which provided a continuous depth calibrated 360° image of the borehole walls. These logs were employed in the construction of a composite depth scale for Smirra 1 and 2. The cores could not be azimuthally oriented at the drill site or after recovery because of the differential rotation of segments and/or single beds within individual cores, a feature probably induced by the shallow inclination of the bedding during rotary coring. Thus, any attempt to manually orient the beds was avoided in order to preserve the integrity of the succession as much as possible. After drilling, the cores were transported to the Royal Netherlands Institute for Sea Research (NIOZ), Texel (The Netherlands), where they were cut longitudinally with a diamond saw blade. For each core, an archive half was obtained and used for non-destructive analyses (i.e. line scan and MS), and a working half for rock sampling. Both core halves are now stored in the sample repository of the Earth Sciences Department of Utrecht University (The Netherlands).

### 3.3. Core scanning data

High-resolution core images and MS data were obtained using the Avaatech XRF Core Scanner II hosted at the NIOZ. Core images were collected by a line scan camera coupled with a linear light source able



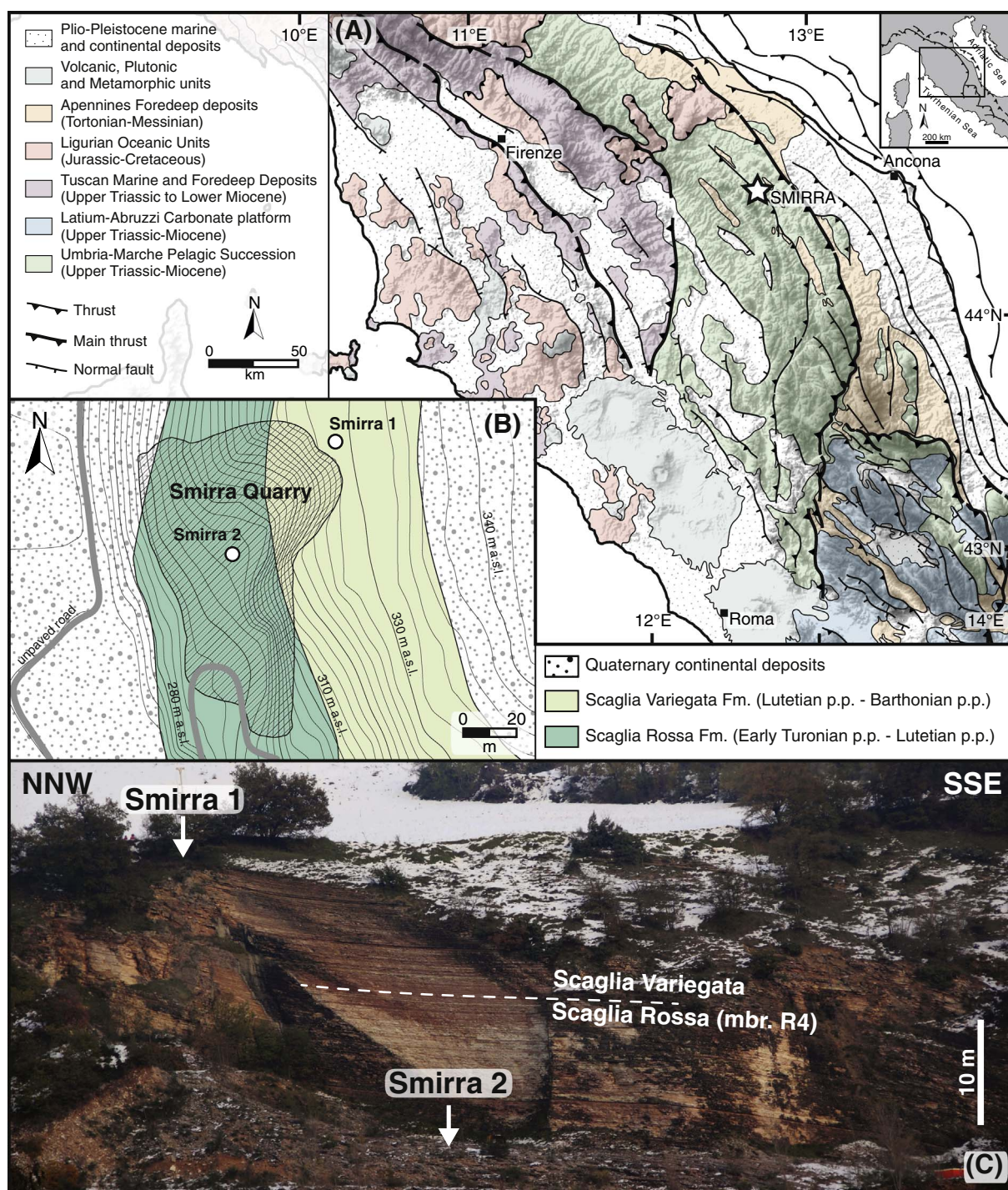


Fig. 1. A) Schematic regional geological map of the Central-Northern Apennines (Italy) with location of the Smirra quarry (white star). B) Detailed geological map (redrawn after “Carta Geologica Regionale – Regione Marche, section 291010 “Pigno”, Scale 1:10000” available on line at <http://www.ambiente.marche.it/Territorio/Cartografieinformazioniterritoriali/Archiviocartograficoeinformazioniterritoriali/Cartografie/CARTAGEOLOGICAREGIONALE110000.aspx>) of the area surrounding the Smirra quarry with location of the Smirra 1 and Smirra 2 drilling holes. C) Photograph of the Smirra outcrop exposing the transition between the Scaglia Rossa Fm. (mbr. R4) and the Scaglia Variegata Fm. (the boundary has been placed in agreement with Franceschi et al., 2015 and our data); the Smirra 1 and Smirra 2 drilling locations are also reported.

to provide accurate color data in both RGB and CIE-lab units with a resolution of  $7 \times 10^{-2}$  mm. The pictures were acquired with a shutter time of 4 s, a lens aperture of 9.5 and a resolution of approximately 150 pixels per cm in cross-core and down-core direction. These images have been used as reference to establish a composite depth scale (see Supplementary Material SM.1) as well as for logging (see Section 4.1). MS was measured using a Bartington MS2E high-resolution point-sensor with a footprint of  $4 \times 10$  mm mounted in the Avaatech XRF Core

Scanner II. Sensor drift correction algorithms are implemented in the Avaatech Magsus acquisition software ([avaatech.com](http://avaatech.com)).

### 3.4. Calcareous nannofossils

In total, 283 samples were collected from Smirra 1 cores 1 to 27 and Smirra 2 cores 1 to 25 (i.e. between 1.79 and 65.99 m composite depth - mcd) for calcareous nannofossil biostratigraphy. From each core, 7–8

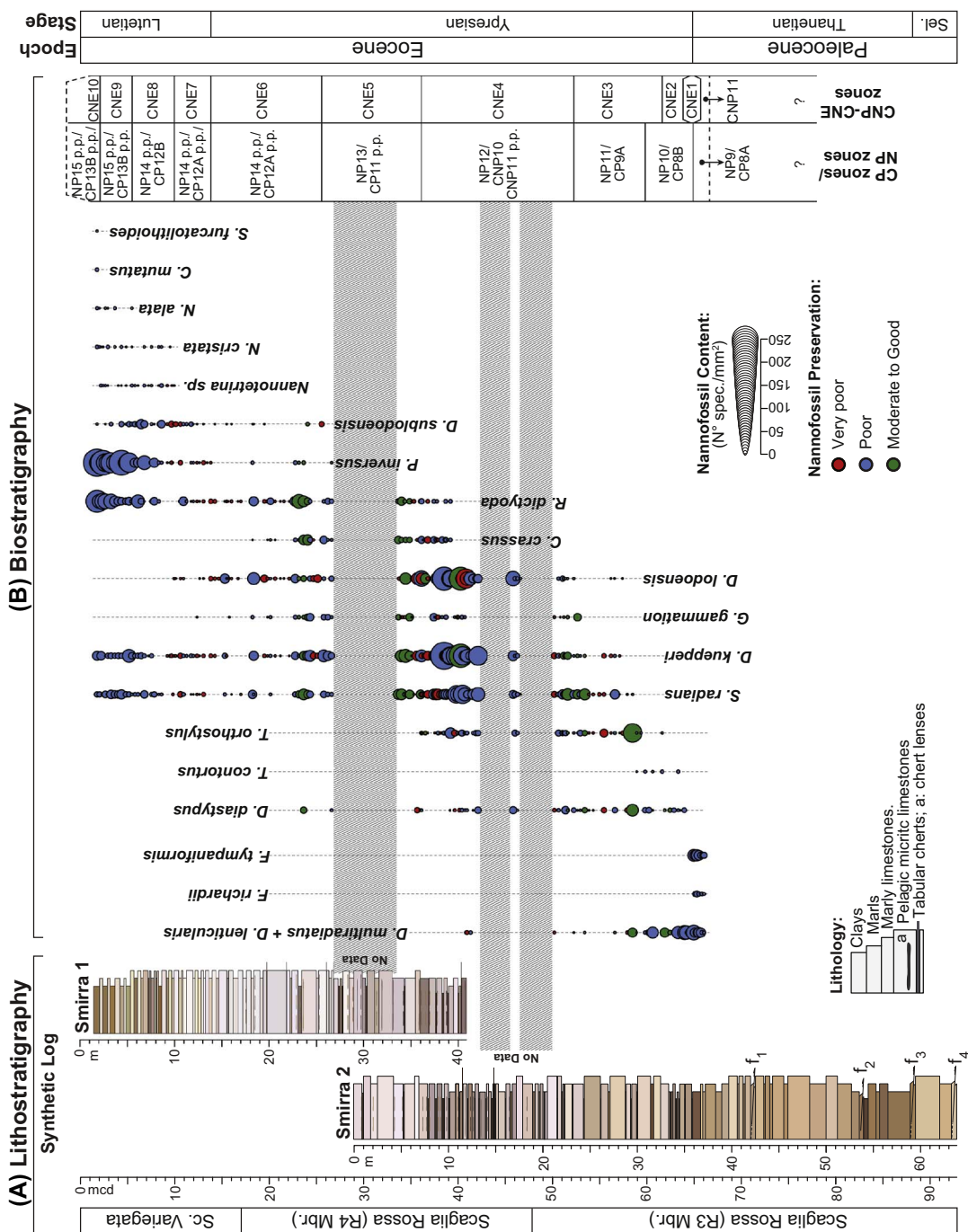


**Fig. 2.** A) Lithostratigraphy (Formation and Member) and synthetic logs (based on the interpretation of coherent lithologic intervals) of the sedimentary succession recovered in Smirra holes 1 and 2. The color of lithology has been inferred from the core line scans. Fault zones ( $f_1$  to  $f_4$ ) are progressively numbered towards the bottom of the section. A detailed overview of the tie points between Smirra 1 and Smirra 2 used to develop the composite depth scale for the whole stratigraphy is provided in Figs. S7 to S12. B) Quantitative biostratigraphy of indicative calcareous nanofossil species identified in the Smirra section. The area of each dot (corresponding to a single-sample biostratigraphic description) is proportional to the N° spec./mm<sup>2</sup>. A sample-by-sample description of the biostratigraphic interpretations is provided in Table S2. (For interpretation of the references to color in this figure legend, the reader is referred to the web version of this article.)



samples were obtained with an average spacing of  $\sim 20$  cm. A total of 185 samples were prepared as smear slides following standard procedures (Bown and Young, 1998). Biostratigraphic analyses were performed with an average resolution of  $\sim 40$  cm, except for intervals close to biozonal boundaries where resolution was increased to  $\sim 10$  cm. The calcareous nannofossil assemblages were studied with a light microscope at a magnification of  $1250\times$  in both plane- and cross-polarized light. The absolute abundance of each taxon was calculated by counting index species on 100 to 300 FOVs (Field of Views) normalized to an area of  $1\text{ mm}^2$  and reported in Table S2.

Preservation varies from moderately good (slightly etched or slightly overgrown forms) to poor and very poor (heavily etched or heavily overgrown forms). Occasionally, poor preservation complicates the identification of some taxa at specific level (e.g. *Tribrachiatulus*, *Nannotetrina* and *Discoaster nannoliths*). The position of biozonal boundaries was calculated as the midpoint between two consecutive samples.

In this study, we used the classic nannofossil biozonations of Martini (1971; i.e. NP) and Okada and Bukry (1980; i.e. CP) as well as the recent biozonal scheme and age estimates proposed by Agnini et al. (2014; i.e. CNP-CNE).

### 3.5. Paleomagnetic and rock-magnetic methods

Paleomagnetic samples were drilled at Utrecht University using a vertical water-cooled driller equipped with a diamond drill bit. In total, 287 paleomagnetic samples were collected from the Smirra 1 and Smirra 2 working halves, collecting on average 4–5 samples from each core with a resolution of  $\sim 30$  cm. The samples were drilled perpendicularly to the vertical core axis and therefore a dip of  $0^\circ$  was assigned to all cylindrical samples as downhole logs indicated that the borehole did not deviate from the vertical by more than  $2\text{--}3^\circ$ . The samples were then cut into standard cylindrical specimens ( $2.5 \times 2.2$  cm) for Natural Remanent Magnetization (NRM) analyses.

In addition, specific rock magnetic analyses were performed on rock-cuttings representative of the different lithologies. The magnetic mineralogy was determined through stepwise Isothermal Remanent Magnetization (IRM) acquisition imparted with an ASC Pulse Magnetizer up to 2.5 T in 25 steps. Six core specimens were also subjected to thermal demagnetization of a three-component IRM (3D-IRM) imparted in 2.5 T, 0.4 T and 0.12 T along three orthogonal directions (Lowrie, 1990). The thermal cleaning procedure is analogous to that applied in the removal of the NRM (see below). The MS during thermal demagnetization of the NRM has also been monitored on representative samples and is reported in SM.3. The MS of all samples was measured using an AGICO KLY-3 Kappabridge.

The NRM of the 287 samples was thermally demagnetized in 15 steps with increments of  $50^\circ\text{C}$  that were reduced to  $20^\circ\text{C}$  after  $500^\circ\text{C}$ . Specimens not completely demagnetized at  $580^\circ\text{C}$  were further heated up to  $675^\circ\text{C}$  with  $25^\circ\text{C}$  increments. The NRM remanence was measured after each heating step using a 2G DC SQUID Cryogenic Magnetometer placed in a magnetically shielded room.

All paleomagnetic measurements were conducted at the Alpine Laboratory of Paleomagnetism (ALP, Peveragno, Italy). NRM demagnetization data were plotted on both orthogonal demagnetization diagrams (Zijderveld, 1967) and equal area projections, and magnetization components were isolated by a principal component analysis (PCA; Kirschvink, 1980) using the Paleomac software (Cogné, 2003).

## 4. Results

### 4.1. Core stratigraphy

The succession recovered in the upper part of Smirra 1 (1.75–17.60 mcd) mainly consists of medium-bedded ( $\sim 15$  cm on average) pink marly limestones with intercalations of reddish marls and

thin clay layers (Figs. 2; S7). This interval corresponds to the basal Scaglia Variegata Fm. (Lutetian p.p.). The underlying unit, reaching 48.00 mcd and well represented in both Smirra 1 and Smirra 2 as a consequence of their overlap, consists of pink and reddish pelagic limestones interbedded with brownish marly-clayey layers (particularly between 36.00 and 44.00 mcd) and cherts (Figs. 2; S8, S9). This interval, which belongs to the R4 member of the Scaglia Rossa Fm. (Ypresian p.p.), is marked by the occurrence of nodular cherts (Arthur and Fischer, 1977; Lowrie et al., 1982). The remaining part of the succession recovered at Smirra 2 is composed of pink to reddish marly limestones and marls (Figs. 2; S10 to S12) and can be attributed to the R3 member (Paleocene) of the Scaglia Rossa Fm. (Arthur and Fischer, 1977). Several brownish marly-clayey layers are present between 48.00 and 65.00 mcd. The lower Paleocene sediments of Smirra 2 are affected by modest tectonic disturbance as a consequence of minor faulting. Finally, the limestone-marl alternations in the Smirra cores are regularly organized in couplets and bundles (see Section 4.6).

### 4.2. Calcareous nannofossil biostratigraphy

Calcareous nannofossil assemblages are generally well diversified (76 taxa recognized and reported in Table S2), and the total abundance varies from a few tens to over 1000 specimens per  $\text{mm}^2$ . Coccoliths, discoasterids and sphenoliths represent the most abundant components of the assemblages throughout the succession. Other taxa are common to abundant in specific intervals of the succession. *Noelaerhabdaceae* (*Cyclicargolithus floridanus*, *Dictyococcites* sp. and *Reticulofenestra dictyoda*) are common to abundant in the upper part together with *Pseudotriquetrorabdulus inversus* and *Zygrhablithus bijugatus*. *Prinsiales* (*Prinsius* and *Toweius*) are common from the lower to middle part of the succession, whereas fasciculiths and holococcoliths (*Octolithus*, *Semihololithus biskayae* and *Zygrhablithus bijugatus*) are common in the lowermost part. Following the reference scheme of Agnini et al. (2014), we identify a continuous succession of 11 calcareous nannofossil biozones ranging from CNP11 to CNE10. Biostratigraphic data and biozonal assignments are summarized in Fig. 2 and in Tables 1 and 2, where indicative taxa, biozones, absolute ages and correlations with Martini (1971) NP zones, Okada and Bukry (1980) CP zones and Agnini et al. (2014) CNP-CNE zones are reported. A detailed description of the calcareous nannofossil biozonation is reported in SM.2.

### 4.3. Rock magnetism

The magnetic properties of the Scaglia Rossa Fm. have been studied for decades (e.g., Lowrie and Alvarez, 1977; Lowrie et al., 1980; Lowrie et al., 1982; Channell et al., 1982) and the reliability of its paleomagnetic record is well established. Our rock-magnetic analysis, therefore, aims to ensure that the magnetic mineralogy of the Smirra core is in agreement with previous studies.

The IRM acquisition curves (Fig. 3A to F) and the results of the thermal demagnetization of the three-component IRMs (Fig. 3G to L) reveal different magnetic behavior as a result of the lithological alternations of pink to red limestones and marly limestones in the Smirra cores.

Throughout the section, the analyzed samples are characterized by both steep (i.e. S2C20\_5; Fig. 3E) and gentle rising IRM acquisition curves, the latter usually showing a moderate increase up to applied fields of  $\sim 0.4\text{--}0.5$  T followed by a modest rise towards 2.5 T (Fig. 3A, B, C, F). This behavior suggests the coexistence of variable amounts of high and low coercivity components. The IRM acquisition curve of the sample S1C07\_8, collected from a brownish marly layer at 37.83 mcd (Fig. 3D), shows the most gradual increase up to 2.5 T without reaching saturation, revealing the presence of a predominant high coercivity component.

The 3D-IRMs show a rather complex pattern with evidence for two discrete unblocking temperatures: one between  $580^\circ\text{C}$ – $600^\circ\text{C}$  and

**Table 1**  
Stratigraphic positions of polarity zones, lithological and nannofossil biozones boundaries.

Lithological boundaries	Nannofossil biozones	Polarity zones (Chron)	Stratigraphic position $\pm$ error (mcd)
Scaglia Variegata/Scaglia Rossa (R4 mbr.)	Base NP15 p.p./CP13b p.p. CNE10		1.92 $\pm$ 0.12
	Base NP15 p.p./CP13a CNE9		5.55 $\pm$ 0.08
	Base NP14 p.p./CP12b CNE8		10.04 $\pm$ 0.07
	Base NP14 p.p./CP12a p.p. CNE7		13.61 $\pm$ 0.20
		Top smi06r (C21r)	11.79 $\pm$ 0.26
			17.00
	Base NP14 p.p./CP12a p.p. CNE6		25.66 $\pm$ 0.11
		Base smi06r (C21r)	24.22 $\pm$ 0.12
		Top smi05r (C22r)	31.56 $\pm$ 0.13
			35.84 $\pm$ 0.18
Scaglia Rossa (R4 mbr.)/Scaglia Rossa (R3 mbr.)	Base NP13/CP11 p.p. base CNE5		37.63 $\pm$ 0.07
		Base smi05r (C22r)	39.17 $\pm$ 0.08
		Top smi04n.1r (C23n.1r)	39.49 $\pm$ 0.08
		Base smi04n.1r (C23n.1r)	44.05 $\pm$ 0.05
		Top smi04r (C23r)	48.00
			49.21 $\pm$ 0.18
	Base NP12/CNP10-CNP11 p.p. base CNE4		52.41 $\pm$ 0.20
		Top smi03n.1r (C24n.1r)	51.83 $\pm$ 0.02
		Base smi03n.1r (C24n.1r)	52.46 $\pm$ 0.10
		Top smi03n.2r (C24n.2r)	53.77 $\pm$ 0.07
		Base smi03n.2r (C24n.2r)	54.18 $\pm$ 0.05
		Top smi03r (C24r)	57.34 $\pm$ 0.06
			61.70 $\pm$ 0.13
	Base CNE3		64.76 $\pm$ 0.06
	Base CNE2		64.89
	Base NP10/CP8B (top NP9/CP8A) base CNE1 (top CNP11)		
		Top smi02r (C25r)	73.95 $\pm$ 0.17
		Base smi02r (C25r)	84.66 $\pm$ 0.20

Correlative polarity chron boundaries are shown in parentheses. Polarity chron nomenclature is after Gradstein et al. (2012). The biozonation is in agreement with Martini (1971; NP zones), Okada and Bukry (1980; CP zones), Agnini et al. (2014; CNP-CNE zones).

another around 675 °C carried by low and mid-high coercivity components, respectively, which are simultaneously present in all analyzed samples. However, the low coercivity component is prevailing in samples S2C17\_2 and S2C27\_2 (Fig. 3J, L), whereas the mid-high coercivity component is dominant in the remaining samples (Fig. 3G, H, I, K).

Our rock-magnetic data are perfectly in agreement with previous classic studies from the Scaglia Rossa Fm. of the Umbria-Marche Basin (e.g., Lowrie and Alvarez, 1977; Lowrie et al., 1980; Lowrie et al., 1982; Channell et al., 1982). Accordingly, we interpret magnetite as the carrier of the low coercivity and low blocking temperature component. On the other hand, the gradually decaying mid-to-high coercivity and high-blocking temperature component can be interpreted as fine-grained pigmentary hematite of (early?) authigenic origin (Tauxe et al., 1980; Dekkers and Linssen, 1989).

#### 4.4. Paleomagnetism

The majority of samples display good quality thermal demagnetization diagrams (Fig. 4A to H). The NRM intensity of the paleomagnetic samples ranges between  $4.35 \times 10^{-5}$  A/m and  $8.42 \times 10^{-3}$  A/m with an average value of  $5.60 \times 10^{-4}$  A/m (Fig. 5). MS values vary between  $2.75 \times 10^{-6}$  SI and  $124.59 \times 10^{-6}$  SI with an average of  $20.80 \times 10^{-6}$  SI (Fig. 5). The highest values of both NRM and MS are found in the red to brown limestones and marly limestones of the Scaglia Rossa Fm. (member R3) located at the base of the succession. The MS shows a progressive decrease towards the top of the section, while the NRM drops almost one order of magnitude (from  $\sim 1.0 \times 10^{-3}$  A/m to  $\sim 3.0 \times 10^{-4}$  A/m) around 50.0 mcd and then remains stable up to top (Fig. 5).

The majority of samples (267 out of 287) is characterized by a low blocking-temperature component with normal polarity and generally removed around 150 °C (Fig. 4A to H, Table S3, Fig. S3A, B). This low temperature normal polarity component shows a mean inclination (computed according to McFadden and Reid, 1982) of  $51.0^\circ \pm 2.7^\circ$  in geographic coordinates, which is close to the Geocentric Axial Dipole

(GAD) field direction expected at the sampling locality ( $D = 0^\circ$ ,  $I = 62.3^\circ$ ). This component might be related to a recent viscous magnetic overprint, also considering that the Meso-Cenozoic sediments of the Umbria-Marche basin are commonly characterized by a similar low-temperature component falling close to the GAD field direction (e.g. Channell et al., 1982; Lanci et al., 1996; Turtù et al., 2013; Satolli et al., 2015; Satolli and Turtù, 2016). The remaining 30 samples exhibit a low-temperature component, also removed around 150 °C, with reverse polarity probably indicating a viscous overprint of a different origin or acquired earlier than the rest of the samples.

Several samples (46 over 287) show an intermediate-temperature component (ITC) in the 150 °C to 250 °C range (Fig. 4D, E, F, Table S4, Fig. S3C) with both normal (4 samples) and reverse polarity (42 samples) and a mean inclination of  $61.6^\circ \pm 4.8^\circ$  in geographic coordinates. A similar reverse polarity ITC in approximately the same temperature range has been isolated from the Marne a Fucoidi (lower Aptian - upper Albian) and the Maiolica Fms. (upper Tithonian - lower Aptian) of the Umbria Marche Basin and interpreted as a post-folding burial-related magnetization of Messinian - early Pliocene age (Satolli et al., 2008 and reference therein). The normal polarity ITC component can be related to similar processes, but acquired at a different time.

A characteristic remanent magnetization (ChRM) component has been identified in 283 (out of 287) samples (98.6%). PCA least-square fitting lines were forced through the origin in 16 samples, corresponding to 5.6% of the whole sample set (Table S5). The NRM of 73% of the samples was usually removed between 500 and 600 °C, which is the typical unblocking temperature range of magnetite (Fig. 4A, E, G, H). The remaining 27% of the samples is fully demagnetized at temperatures ranging from 600 up to 675 °C (Fig. 4B, C, D, F), in agreement with the presence of (fine-grained) hematite inferred from rock magnetic analyses (see Section 4.3).

In thermal demagnetization experiments of Upper Cretaceous - lower Paleocene Scaglia Fm. samples positioned at reversal boundaries, Channell et al. (1982) documented the presence of primary magnetization components followed, at higher temperature, by antipodal

**Table 2**  
Stratigraphic position and age of calcareous nannofossil key biohorizons at Smirra.

Biohorizon	Nannofossil biozone	Sample	Error ( ± , m)			Chron	Fract. pos. (%)	Age, Ma ( ± error, Ma)	
			Base (mcd)	Top (mcd)	Mean (mcd)			GPTS2012	GPTS2004
<i>B. S. furcata</i> <i>lenticularis</i>	CNE10 (?)	2.05	1.79	1.92	1.92	C21n (?)	–	–	–
<i>B. C. mutans</i>	CNE10 (?)	2.05	1.79	1.92	1.92	C21n (?)	–	–	–
<i>T. Nannoterina</i> sp.	CNE9	2.21	2.05	2.13	2.13	C21n (?)	–	–	–
<i>B. N. alata</i>	CNE9	5.62	5.47	5.55	5.55	C21n	–	–	–
<i>B. N. cristata</i>	CNE8	9.66	9.51	9.59	9.59	C21n	–	–	–
<i>B. Nannoterina</i> sp.	CNE8	10.11	9.96	10.04	10.04	C21n	–	–	–
<i>T. D. lodoensis</i>	CNE7	10.11	9.96	10.04	10.04	C21n	–	–	–
<i>T. D. gannation</i>	CNE7	12.63	12.36	12.50	12.50	C21n	–	–	–
<i>HCO D. lodoensis</i>	CNE7	13.82	13.41	13.61	13.61	C21r	5.71	47.42 (0.014)	47.31 (0.015)
<i>LCO T. inversus</i>	CNE7	13.82	13.41	13.61	13.61	C21r	14.64	47.53 (0.020)	47.43 (0.022)
<i>T. C. crassus</i>	CNE6	18.35	18.23	18.29	18.29	C21r	52.29	47.53 (0.020)	47.43 (0.022)
<i>T. D. diastypus</i>	CNE6	24.06	23.64	23.85	23.85	C21r	97.02	47.99 (0.006)	47.95 (0.007)
<i>B. D. subloensis</i>	CNE6	25.77	25.55	25.66	25.66	C22n	19.62	48.53 (0.021)	48.56 (0.023)
<i>T. T. orthostylus</i>	CNE5	36.01	35.66	35.84	35.84	C22r	70.51	48.72 (0.012)	48.76 (0.012)
<i>B. R. dictyoda</i>	CNE4	39.37	39.17	39.27	39.27	C23n.1r	32.25	50.25 (0.038)	50.35 (0.039)
<i>B. C. crassus</i>	CNE4	39.37	39.17	39.27	39.27	C23n.1r	32.25	50.87 (0.042)	50.97 (0.040)
<i>T. D. multiradiatus</i> + <i>D. lenticularis</i>	CNE4	40.79	40.70	40.75	40.75	C23n.2n	27.79	50.87 (0.042)	50.97 (0.040)
<i>LCO D. lodoensis</i>	CNE4	52.60	52.21	52.41	52.41	C24n.1r	92.06	51.29 (0.007)	51.29 (0.007)
<i>B. G. gannation</i>	CNE3	52.90	52.60	52.75	52.75	C24n.2n	22.14	53.19 (0.041)	53.11 (0.036)
<i>B. D. kuepperi</i>	CNE3	57.44	57.07	57.26	57.26	C24n.3n	94.48	53.22 (0.008)	53.13 (0.006)
<i>B. D. lodoensis</i>	CNE3	57.87	57.44	57.66	57.66	C24r	–	53.95 (0.031)	53.78 (0.029)
<i>LCO D. multiradiatus</i> + <i>D. lenticularis</i>	CNE3	58.87	58.43	58.15	58.15	C24r	–	–	–
<i>T. T. contortus</i>	CNE3	58.88	58.43	58.66	58.66	C24r	–	–	–
<i>B. S. radians</i>	CNE3	58.88	58.43	58.66	58.66	C24r	–	–	–
<i>B. T. orthostylus</i>	CNE3	61.83	61.56	61.70	61.70	C24r	–	–	–
<i>B. T. contortus</i>	CNE2	63.47	63.26	63.37	63.37	C24r	–	–	–
<i>B. D. diastypus</i>	CNE2	63.93	63.90	63.92	63.92	C24r	–	–	–
<i>T. F. tympaniformis</i>	CNE1	65.02	64.90	64.96	64.96	C24r	–	–	–
<i>T. F. richardii</i>	CNE1	65.02	64.90	64.96	64.96	C24r	–	–	–

The age (in Ma) of bioevents was computed according to the correlation between the Smirra magnetostratigraphy and the polarity record from GPTS2012 (Gradstein et al., 2012), GPTS2004 (Gradstein et al., 2004) and CK95 (Cande and Kent, 1995).

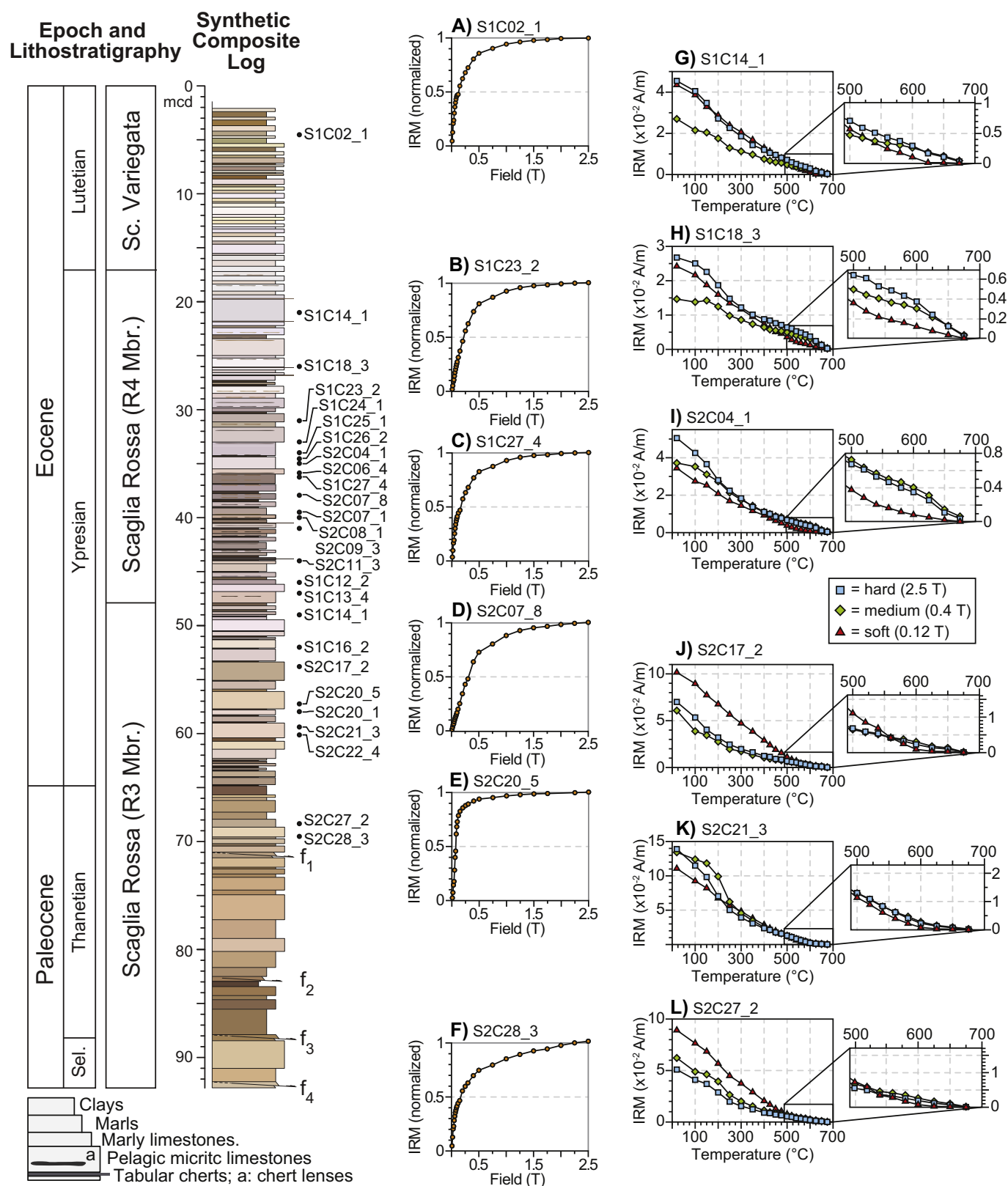


Fig. 3. Rock magnetism experiments for representative samples of the Smirra section. A–F) Isothermal Remanent Magnetization (IRM) acquisition curves (normalized); G–L) thermal unblocking features of orthogonal axis IRMs.

components. The carriers of these components have been interpreted, respectively, as detrital (or biological) magnetite and diagenetic (post-polarity reversal) hematite originating from a goethitic precursor. This mechanism, acting via haematite growth through single-domain critical

volume prior to mechanical fixation of magnetite, is responsible for recording polarity reversals at different stratigraphic levels (Channell et al., 1982).

The thermal demagnetization diagrams of samples located at



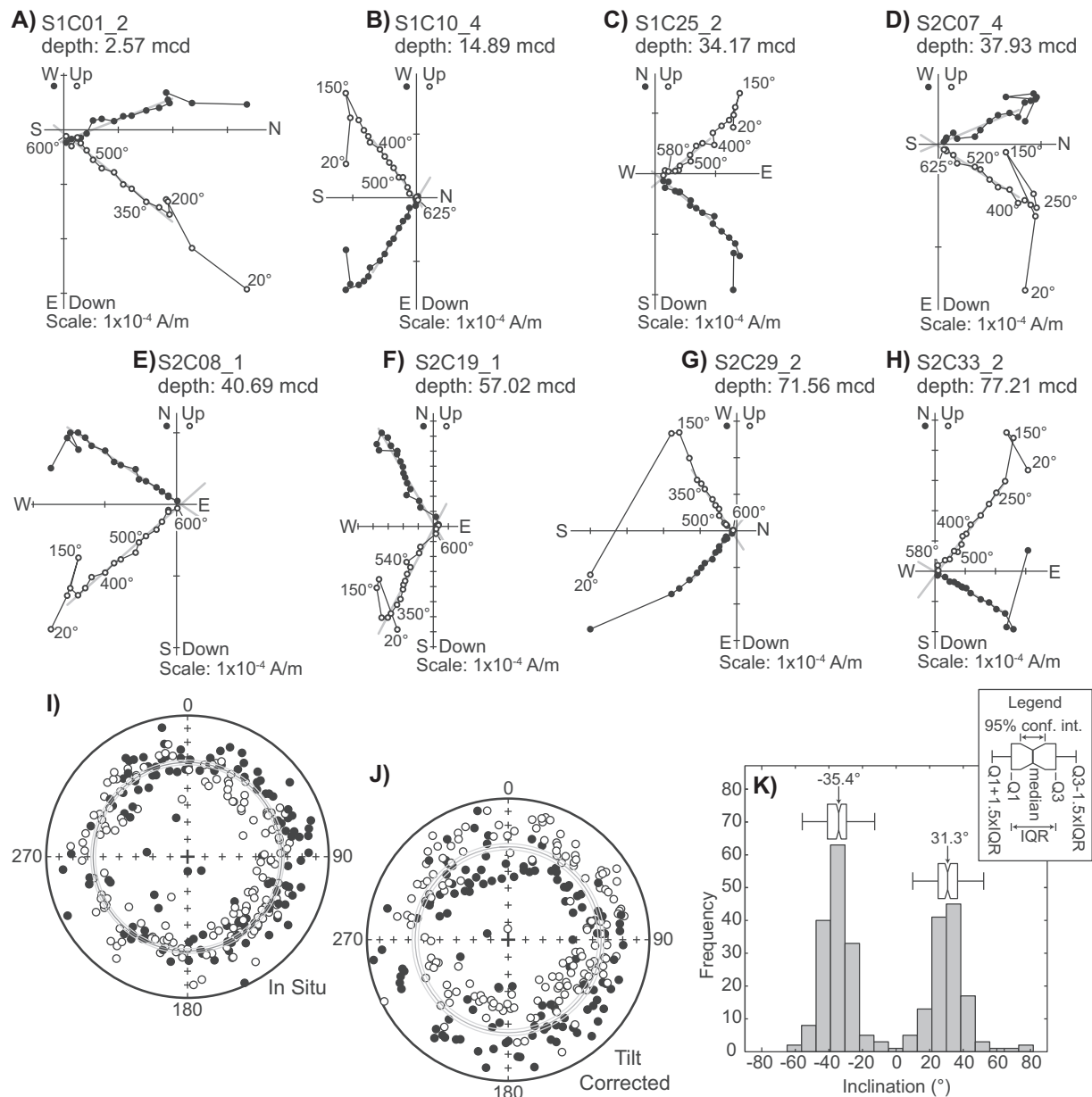


**Fig. 4.** Paleomagnetic analysis results. A–H) Vector diagrams of demagnetization data, in situ coordinates. Closed circles are projections onto the horizontal plane and open circles are projections onto the vertical plane. Data were obtained by thermal demagnetization; demagnetization step values are expressed in °C. Light grey lines represent the interpreted ChRM component. Sample location: A, B) Scaglia Variegata Fm.; C, D, E) Scaglia Rossa Fm. (member R4); F, G, H) Scaglia Rossa Fm. (member R3). I, J) Equal-area projections of the ChRMs for the Smirra section. Solid (open) circles represent projections onto the lower (upper) hemisphere. Dark grey circles represent the mean inclination with error bounds (in light grey) according to [McFadden and Reid \(1982\)](#). K) Histogram of inclinations and box plots (with median values) of the positive and negative inclination, in situ coordinates. The notch in each box plot represents the 95% confidence interval while the end of the “whiskers” has been set to 1.5 of the interquartile range (IQR), representing the lowest and the highest datum still within 1.5 IQR of the lower (Q3) and upper (Q1) quartile, respectively, which corresponds to approximately  $2.7\sigma$  of the data coverage.

reversal boundaries in the Smirra section are characterized by ChRMs showing a linear trend towards the origin of the demagnetization diagram, generally from 300 to 350 °C up to the unblocking temperature range of magnetite (500–600 °C) and hematite (600–675 °C). However, these samples do not show the complex behavior, such as antipodal components, observed by [Channell et al. \(1982\)](#). This implies that the magnetite and the diagenetic hematite recorded their magnetization at roughly the same time, possibly as a result of an increase in sedimentation rate during the Paleocene to Eocene. A higher sedimentation rate is, in fact, considered to affect the concentration of goethite and hence the duration of hematite growth ([Channell et al., 1982](#)).

ChRM directions plotted on equal area projection before and after tilt correction (Fig. 4I, J) clearly show the loss of azimuthal orientation

of the paleomagnetic cores due to drilling. In fact, the declination of samples with both positive and negative inclination are spread around the stereographic projections. The overall paleomagnetic mean direction (in normal polarity) computed by [Franceschi et al. \(2015\)](#) for the upper Ypresian - lower Lutetian sediments in the Smirra quarry is  $D = 52.0^\circ$ ,  $I = 45.6^\circ$ ,  $n = 21$ ,  $\alpha_{95} = 6.5^\circ$ ,  $k = 19.9$ . Only a small group of samples appears to be in agreement with this direction, while it is not possible to confirm the correct orientation of the remaining part of the samples. On the other hand, the mean inclinations (computed according to [McFadden and Reid, 1982](#)) are well clustered around  $33.6^\circ \pm 1.5^\circ$  in geographic coordinates and more scattered in tilt corrected projection, although characterized by a similar mean inclination ( $34.5^\circ \pm 2.0^\circ$ ).

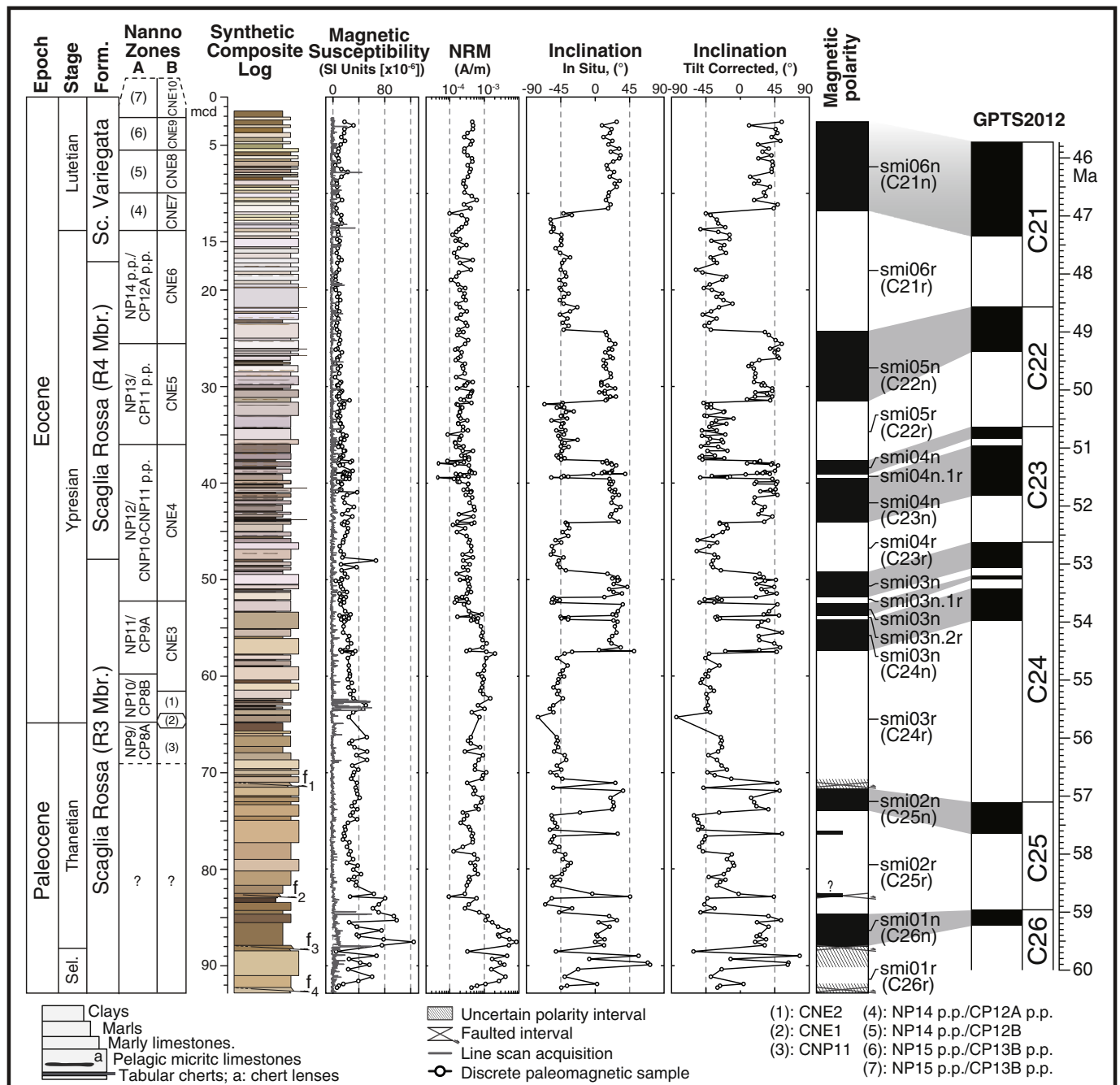
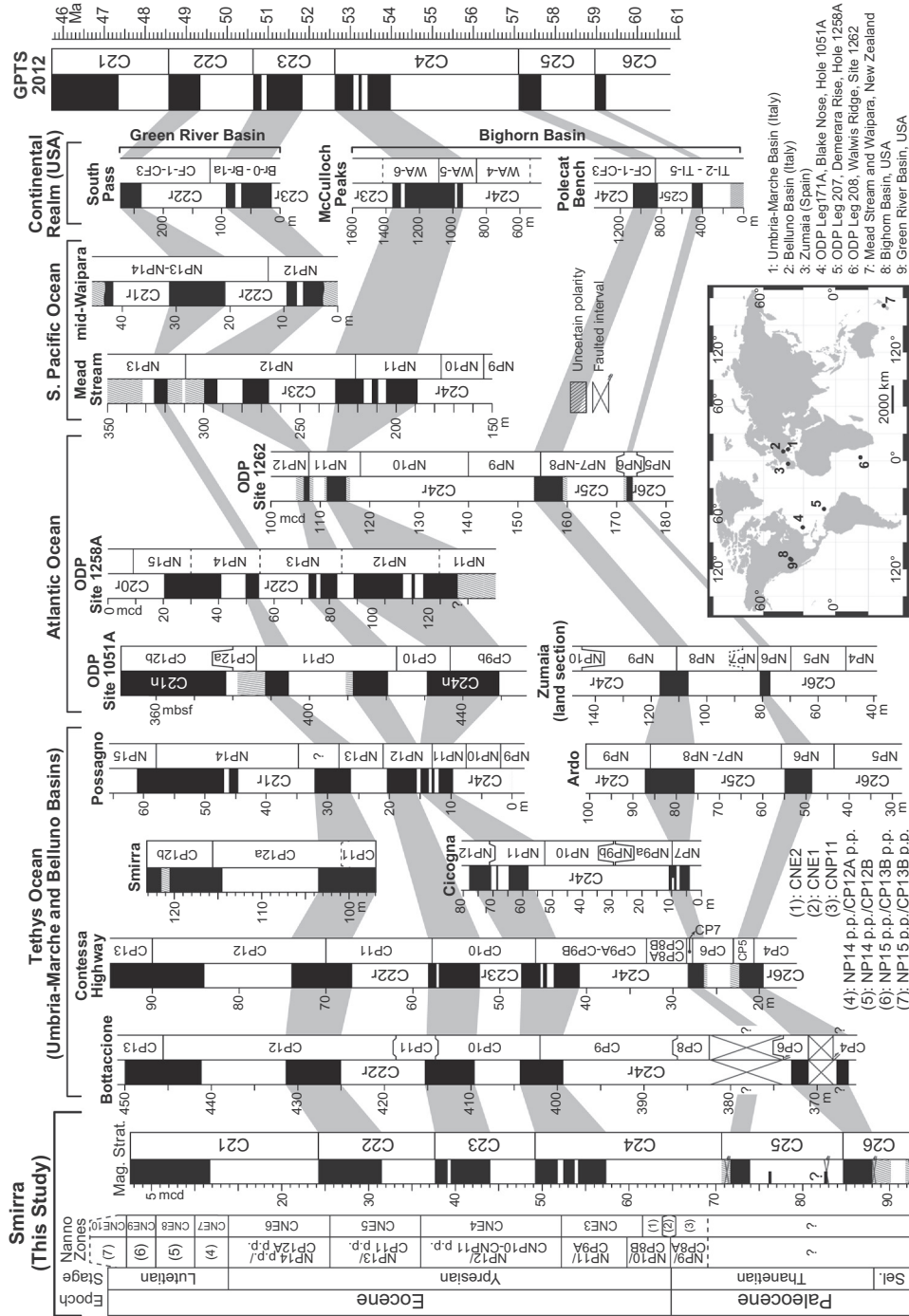


Fig. 5. Magnetic stratigraphy of the Smirra section summarizing the stratigraphic variations of magnetic susceptibility (from both line scan acquisition and discrete paleomagnetic samples), NRM and Inclination (in both in situ and tilt corrected coordinates). The magnetic declination is not reported as not useful to constrain the magnetic polarity stratigraphy due to the uncorrected azimuthal orientation of the samples (see text for explanation). The magnetic polarity zones (black for normal polarity, white for reverse polarity) and subzones are progressively numbered from the section bottom. The correlation with the GPTS2012 is also indicated.

Several lines of evidence support a primary nature of the ChRMs despite the impossibility of performing reliability tests. (1) A histogram of inclinations (Fig. 4K) shows a clear separation into two, almost opposite, modes and compares well with box plots for the up- and down-pointing ChRM inclinations (Fig. 4K). The median values (with corresponding 95% confidence boundaries) are  $31.3_{33.3}^{29.2}$  and  $-35.4_{-34.0}^{-36.8}$  for positive and negative inclinations, respectively. (2) No indications for regional remagnetization have so far been reported from the Meso-Cenozoic succession in the Umbria-Marche Basin (e.g. Speranza et al., 2005), whereas a fully reliable primary magnetization has been found in the Smirra quarry (Franceschi et al., 2015). (3) The ChRMs show both positive and negative inclinations that

correspond to both normal and reversed polarity intervals. (4) The average inclinations at Smirra are rather similar to the inclinations for the Paleocene ( $\sim 39^{\circ}$ ) and Eocene ( $\sim 41^{\circ}$ ) portions of the Contessa section (Lowrie et al., 1982). A larger difference is found with both the mean inclination ( $I = 45.6^{\circ}$ ) computed by Franceschi et al. (2015) and the inclination expected at Smirra coordinates ( $I = 59.1$ ) by the African APWP of Besse and Courtillot (2002). However, the potential influence of inclination shallowing of primary ChRM directions and/or a partial tilt correction at Smirra due to azimuthal misorientation must be taken into account in this comparison. (5) The mean inclination is only slightly varying with depth in both geographic ( $\pm 10.3^{\circ}$ ) and stratigraphic ( $\pm 13.5^{\circ}$ ) coordinates (Fig. 4). For these reasons, the



**Fig. 6.** Correlation (redrawn and updated after Dallanave et al., 2015) between the magneto-bio-stratigraphy of the Smirra section and representative records from the Tethys, Atlantic and Pacific Ocean domains as well as from the north American continental realm (i.e. Bighorn and Green River Basins). For each locality the bio-magnetostratigraphic records refer to: Bottaccione (Lowrie et al., 1982; Napoleone et al., 1983; Monetti and Thierstein, 1985), Contessa Highway (Lowrie and Alvarez, 1977; Lowrie et al., 1982; Napoleone et al., 1983; Monetti and Thierstein, 1985; Galeotti et al., 2000; Jovane et al., 2007; Galeotti et al., 2010; Corconi et al., 2012), Cicogna (Dallanave et al., 2009); Possagno (Agnini et al., 2006), Ardo (Dallanave et al., 2012), Smirra (Franceschi et al., 2015), ODP Site 1051A (Ogg and Bardot, 2001; Edgar et al., 2010), ODP Site 1258A (Suganuma and Ogg, 2006; Edgar et al., 2010), ODP Site 1262 (Bowles, 2006; Agnini et al., 2007; Westerhold et al., 2008), Zumaia (Dinarès-Turell et al., 2002, 2003, 2007), Mead Stream (Dallanave et al., 2015), mid-Waipara River (Dallanave et al., 2016), South Pass section (Clyde et al., 2001), McCulloch Peaks (Clyde et al., 1994), Polecat Bench (Butler et al., 1981). The records from Smirra and the Bottaccione – Contessa Highway are drawn in the same vertical scale to facilitate comparison. The biozonations of Martini (1971; NP), Okada & Bukry (1980; CP) and Agnini et al. (2014; CNP-CNE) are adopted in the marine sections. The biozones for the continental sections refer to The North American Land Mammals Age (NALMA) framework. (e.g. Butler et al., 1981; Clyde et al., 1994; Clyde, 2001). The inset shows the location of the sections used for the correlation.



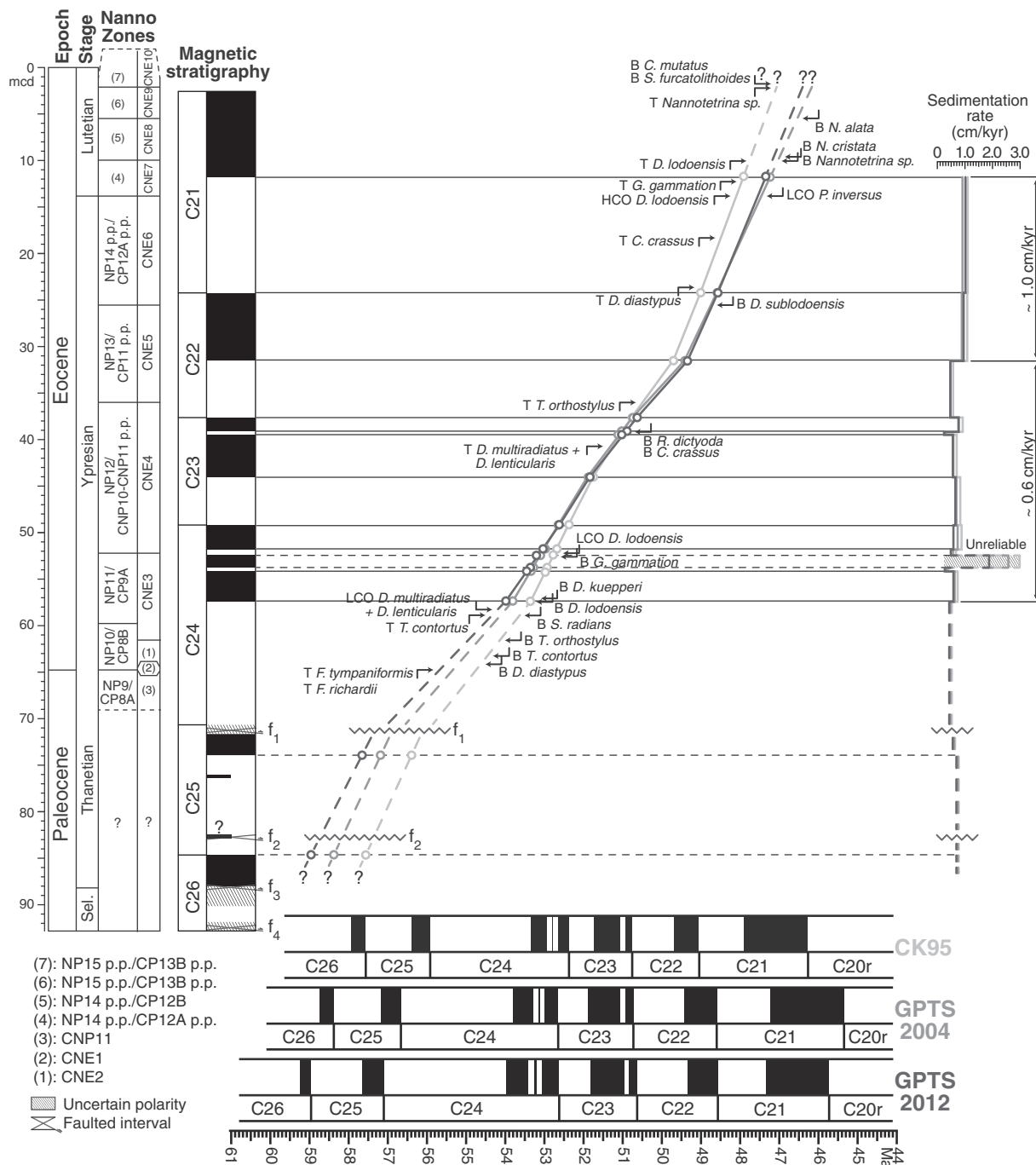


**Fig. 7.** Stratigraphic distance vs. age correlation plot. The magnetic polarity zones of the Smirra section are correlated to the reference polarity sequence from the GPTS2012 (Gradstein et al., 2012), GPTS2004 (Gradstein et al., 2004) and CK95 (Cande and Kent, 1995) time scales. The sloping lines are the average sediment accumulation rates. On the right, the sedimentation rates, computed according to each correlation option, are reported in cm/kyr. Calibrated calcareous nannofossil key biohorizons are also indicated (B: base, LCO: lowest common occurrence, HCO: highest common occurrence, T: top).

paleomagnetic data collected at Smirra can be considered reliable enough for defining an inclination-only magnetostratigraphy.

#### 4.5. Magnetobiostratigraphic age model

Magnetic inclinations define a succession of normal- and reverse-polarity magnetozones numbered in stratigraphic order from the bottom to the top of the succession (Fig. 5, Table 1). The paleomagnetic results, integrated with biostratigraphic data, allow to calibrate the magnetic stratigraphy to the recent GPTS2012 (Figs. 5, 6). From the top of the section to ~70.0 mcd, the pattern of magnetozones is continuous

and can be unambiguously correlated to magnetochrons C21n to C24r. Below ~70.0 mcd, minor faults, marked by clear shear zones, interrupt the continuity of the succession. As a result, the polarity sequence is less easy to interpret although the presence of Chrons C25 and (part of) Chron C26 could reasonably be inferred.

Age-depth plots were used to reconstruct the sedimentation history of the Smirra cores (Fig. 7). They are based on correlating the Smirra magnetic polarity stratigraphy to CK95 as well as with GPTS2004 and GPTS2012. The tie points originate from the 13 reversal boundaries that correspond to Chrons C21n to C24r. The base of Chron C25n and the top of Chron C26n have also been tentatively indicated. Sediment

accumulation rate curves were generated for each correlation option with sedimentation rates assumed to be constant between tie points (i.e. for each polarity (sub)chron). According to the different polarity time scales, sedimentation rates vary minimally between 1.09 cm/kyr (CK95), 0.98 cm/kyr (GPTS2012) and 0.9 cm/kyr (GPTS2004) for the top part of the succession (C22n to C21r). From the base of C24n to C22r, sedimentation rates reveal a general increase (0.65 to 0.5 cm/kyr), with estimates similar to those ( $\sim 0.65$  cm/kyr on the average) inferred for the lower part of the succession (C26r to C24r).

The age model derived by polarity correlation has been used to calibrate the calcareous nannofossil biohorizons (Fig. 7) and derive the age of bioevents between C21r and C24n, according to the most recent GPTS2012 as well as to older time scales (i.e. GPTS2004 and CK95) (Table 2).

#### 4.6. Cyclostratigraphy

We used variations in the high-resolution MS record as an independent mean to assess sedimentation rates in the Smirra cores by assuming that these variations are astronomically controlled. MS can be considered as a proxy for carbonate content, reflecting orbitally induced variations in carbonate production/dissolution and/or siliciclastic dilution (Reynolds and King, 1995; Ellwood et al., 2000).

For this purpose, we employed wavelet analysis in the depth domain (Torrence and Compo, 1998) in combination with Evolutive Harmonic Analysis (EHA) and Evolutive Power Spectral Analysis (EPSA) (Meyers et al., 2001; Meyers and Hinnov, 2010) of the MS between Chrons C21n and C24r (Figs. 8C, S4). This combination of statistical methods was applied to evaluate cyclic changes in spatial bedding. The outcome reveals the presence of two dominant cycle components, a small-scale and a large-scale component with periods of 0.6 to 0.8 m and 2.5 to 5.0 m, respectively. According to the average sedimentation rates estimated from our initial magnetostratigraphy-based age models (Fig. 8C), we interpret these periodicities to represent the imprint of the short (E2–E3 = 96–125 kyr) and long (E1 = 405 kyr) eccentricity cycles. Significant but discontinuous peaks with periods of  $\sim 0.3$  m and  $\sim 0.2$  m could additionally be correlated to obliquity (O =  $\sim 41$  kyr) and precession (P =  $\sim 21$  kyr). The power of the  $\sim 2.5$  m and 4 m cycles remains relatively stable throughout the record, except for the interval between  $\sim 33$  and  $\sim 44$  mcd, where the signal is weaker. Moreover, in the upper interval, the power is more strongly concentrated around  $\sim 5$  m and  $\sim 0.8$  m, suggesting an upward increase in sedimentation rate (Figs. 8C, S4).

This evidence for the presence of astronomically controlled cyclicity paves the way for an independent test of our initial age models using the evolutive Average Spectral Misfit method (e-ASM; Meyers and Sageman, 2007; Meyers et al., 2012). This method provides an objective estimate of the optimal sedimentation rate for a stratigraphic interval that contains a record of orbital forcing. Using the results of EHA and EPSA, and the initial age models (Fig. 7) as constraints, e-ASM analysis was performed to evaluate a range of possible sedimentation rates for the Smirra cores (Fig. 8D, E). Within Chron C24n, e-ASM indicates a sedimentation rate varying between  $\sim 0.67$  and  $0.82$  cm/kyr (on average). Similarly, the sedimentation rate during Chron C23r is also slightly variable ( $\sim 0.7$  cm/kyr on average). Nevertheless, this rate is highly significant ( $H_0$ -SL = 0.2%) in the interval around 47 mcd, suggesting a stable accumulation rate of  $0.65$  cm/kyr (Fig. 7). Upcore, the interval across Chrons C23n and C22r is characterized by ambiguous results, probably as a consequence of a lower signal-to-noise ratio associated with the decrease in significance of the E1 harmonic term in the MS record (Figs. 8, S4). To overcome this complication, we applied the adaptation of the ASM method (Meyers and Sageman, 2007) developed by Ma et al. (2014) (Figs. 8E, S5, S6), which is useful in case a relatively weak but continuous orbital signature is preserved. As a result, we derived an optimal sedimentation rate of  $0.63$  cm/kyr ( $ASM = 5.24 \times 10^{-4}$  cycles/kyr,  $H_0$ -SL = 2.02%) for Chron C23n.2n

and of  $0.64$  cm/kyr ( $ASM = 6.5 \times 10^{-4}$  cycles/kyr,  $H_0$ -SL = 1.86%) for Chron C22r. The average sediment accumulation rates for Chrons C22n and C21r vary from  $\sim 1.07$  to  $\sim 1.14$  cm/kyr, respectively. This is consistent with the observed increase in cycle thickness in the upper part of the core.

## 5. Discussion

### 5.1. Magnetostratigraphic correlation

The magnetostratigraphic record of the Smirra cores allows a detailed correlation with coeval land-based and deep-sea records (Fig. 6). The correlation encompasses several reference sections from the Tethyan Umbria-Marche and Belluno basins, including the Smirra outcrop studied by Franceschi et al. (2015). The correlation has further been extended to ODP records from the Atlantic Ocean, land-based sections from the Pacific Ocean (i.e. Mead Stream and mid-Waipara River) and the continental realm of North America. The correlation panel shows a general agreement in polarity chrons and nannofossil biozones on a global scale.

In particular, magnetostratigraphic records from the Umbria-Marche Basin are consistent with the Smirra cores and the relative thickness difference between polarity chrons is generally limited. A larger discrepancy is only observed for Chron C22r, where slightly larger relative difference are found between Smirra and the Contessa-Bottaccione sections. Moreover, subchron C24n.2n is relatively thick at Smirra compared to other sections and cores (e.g. Contessa, Cicogna, and ODP Site 1258A), where it is usually thinner than the bounding reversed C24n.1r and C24n.2r subchrons (Fig. 6). These differences might be related to an undetected tectonic deformation even though no evidence of faulting was observed in the cores and optical logs. On the other hand, subchron C23n.1r, which was not detected in several reference localities (e.g. Possagno, ODP Site 1262, Mead Stream), has been identified at Smirra and its relative position is comparable with other records (e.g. Contessa, ODP Site 1258A, mid-Waipara River).

### 5.2. Calibration of bioevents and biochronology

The age-calibrated nannofossil bioevents, derived according to our magnetostratigraphic age model (Fig. 7), allow a comparison with the latest GPTS2012 as well as with previous nannofossil biozonation schemes (e.g. Agnini et al., 2014, based on CK95) (Table 2). The position of the bioevents in the Smirra cores relative to the magnetostratigraphic framework is in overall good agreement with existing records from other locations for the same time interval (Fig. 7), confirming the high quality of this magnetobiostratigraphic framework.

Starting from the top of the succession, the presence of *Sphenolithus furcatolithoides* at  $1.92 \pm 0.13$  mcd indicates proximity close to the boundary between Chrons C20r and C21n, as the B of *Nannotetrina alata* at  $5.55 \pm 0.08$  mcd is usually associated with the upper part of Chron C21n. The B of *Nannotetrina cristata* ( $9.59 \pm 0.08$  mcd), *Nannotetrina* sp. ( $10.04 \pm 0.07$  mcd) and the T of *Discoaster lodoensis* ( $10.04 \pm 0.07$ ) correspond with the lowermost portion of Chron C21n. The stratigraphic position of these events is in partial disagreement with reference records (e.g. Possagno section; Agnini et al., 2006, 2014). Considering that poor preservation hampered the precise portrayal of this interval, a better match is obtained if we consider the HCO of *D. lodoensis* ( $13.61 \pm 0.20$  mcd) in the uppermost part of Chron C21r. According to Backman (1986), the coincidence with the LCO of *Pseudotriquetrorhabdulus inversus* is a further indicator for the proximity of the T of *D. lodoensis*. The B of *Discoaster subloensis* ( $25.66 \pm 0.11$  mcd) has been used to constrain the base of biozone CNE6 (Figs. 2, 7; S2) in the uppermost portion of C22n and our results are in fair agreement with the records from both Possagno (Agnini et al., 2006, 2014) and Contessa (Coccioni et al., 2016). The T of *Tribrachiathus orthostylus* ( $35.84 \pm 0.18$  mcd) is located in the lower part

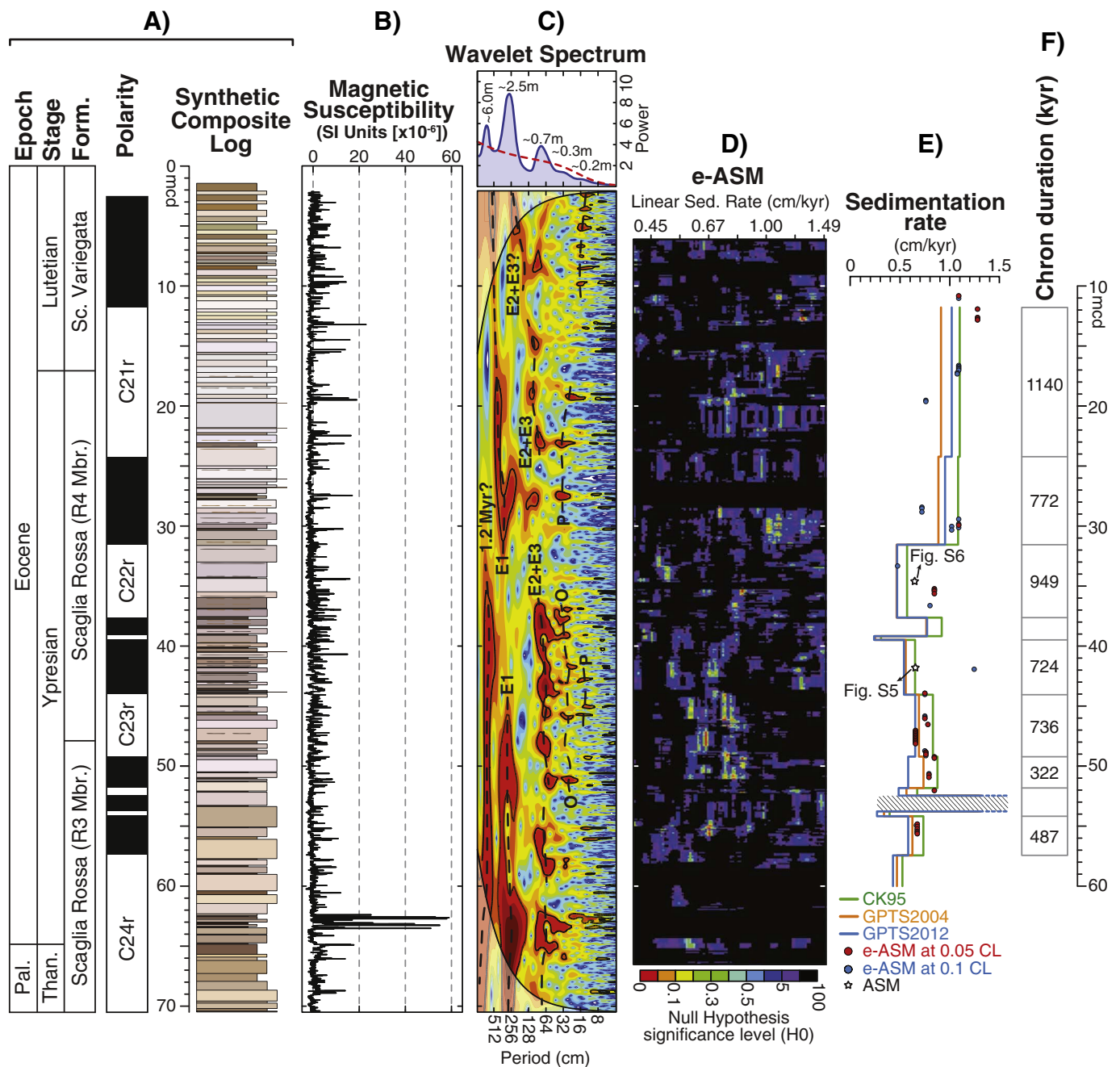


**Fig. 8.** Astronomical testing of the Smirra section. A) Litho- and magneto-stratigraphy (see Figs. 2, 5 for details). B) Wavelet analysis for the high-resolution magnetic susceptibility record (B) in depth domain using a Morlet mother wavelet of an order of 6; the shaded area represents the 95% confidence level; spectral power above the confidence level is concentrated at distinct frequencies. C) Evolutive Average Spectral Misfit (e-ASM) analysis results of EHA (see Fig. S3 for computing details) spectral maxima exceeding the probability threshold of 0.8. e-ASM parameters: Rayleigh frequency = 0.125 cycles/m, Nyquist frequency = 7 cycles/m, evaluating 100 sedimentation rates from 0.4 to 1.5 cm/kyr, with log-scaling for the grid and 100,000 Monte Carlo simulations; orbital targets are from Laskar et al. (2004). D) Comparison between the age models of sedimentation derived from correlation with GPTSs and the e-ASM results with null hypothesis significance levels ( $H_0$ -SL)  $\leq 0.5\%$  (red dots) and  $\leq 1.0\%$  (blue dots) as well as the results of ASM analysis (stars) performed according to Ma et al. (2014) (see Figs. S4 and S5 for details). E) Chron durations derived by the (e-)ASM analysis (see also Table S6). (For interpretation of the references to color in this figure legend, the reader is referred to the web version of this article.)

of Chron C22r in a similar stratigraphic position as in Contessa (Coccioni et al., 2016) and mid-Waipara River (Dallanave et al., 2016), and in a slightly higher position than in Possagno (Agnini et al., 2006, 2014), while the B of both *Coccolithus crassus* and *Reticulofenestra dictyoda* ( $39.27 \pm 0.10$  mcd) fall within Chron C23n.1r. At Possagno (Agnini et al., 2006, 2014), where subchron C23n.1r was not identified, the B of *C. crassus* was recorded in a similar relative position as at Smirra (within a  $\sim 50$  kyr age difference) and thus represents a reliable indicator for Chron C23n. The LCO of *D. lodoensis* ( $52.41 \pm 0.20$  mcd) at Smirra correlates with the base of Chron C24n.1r, while it has been

found in the lowermost C24n.1n in the Cicogna section (Dallanave et al., 2009). On the other hand, specimens of cf. *D. lodoensis* encountered down to 57.44 mcd could mark the B of *D. lodoensis* ( $57.66 \pm 0.22$ ) around the base of Chron C24n.3n, in good agreement with data from Cicogna section. Downsection, the B of *Sphenolithus radians* ( $58.66 \pm 0.23$  mcd), *T. orthostylus* ( $61.70 \pm 0.13$  mcd) and *D. diastypus* ( $63.92 \pm 0.02$  mcd) denote a link to Chron C24r. The T of both *Fasciculithus tympaniformis* and *Fasciculithus richardii* ( $64.96 \pm 0.06$  mcd), in particular, located around the top of a reddish marly interval, suggests the presence of the Paleocene-Eocene



Boundary. This interpretation is supported by data from ODP Site 1262 (Agnini et al., 2007, 2014) and by the appearance of *Tribachiatius bramlettei* above the marly interval (at  $64.21 \pm 0.10$ ; see Table S2), in agreement with observations from the Contessa section (Galeotti et al., 2010).

### 5.3. Sedimentation rates and implications for the geologic time scale

Our age models have been used in combination with the results of the cyclostratigraphic analysis to reconstruct the Smirra depositional history and evaluate potential implications for the geologic time scale. The overall sedimentation rates calculated for the Smirra cores are comparable with estimates from coeval sections in the Umbria-Marche Basin (Lowrie et al., 1982; Galeotti et al., 2010; Coccioni et al., 2013). However, according to these correlations, the sedimentation rates appear quite variable in Chron C23n and particularly within subchron C24n.2n (Figs. 7, 8). In the first case, the reason for these variations in the estimate of sedimentation rate might be related to uncertainties that still affect the ages of Chron C23n in GPTS2012 (Vandenbergh et al., 2012). These discrepancies may derive from the quality of the records on which the astronomical age models are based (Vandenbergh et al., 2012), but also from the accuracy of reference magnetic anomaly profiles (e.g. Cande and Kent, 1992) and the absolute ages of radio-isotopic tie points (Westerhold et al., 2015). In fact, spreading rates based on CK95 reveal sharp variations between C23n.2n and C23r within three different oceanic basins (Bouligand et al., 2006), suggesting a different relative duration of these (sub)chrons. However, this may also reflect potential issues with the synthetic anomaly profile (Cande and Kent, 1992) that was used as a reference in Cande and Kent (1995) and Vandenbergh et al. (2012) to build their geologic time scales for this interval of time. On the other hand, we consider the sedimentation rate increase observed in Chron C24n.2n unreliable. This discrepancy is likely not related to uncertainties in the time scale and seems to result from an anomalous thickness of this polarity interval at Smirra, as compared to other sections and cores.

The results of the (e-)ASM analysis provide an independent estimate of the optimal sedimentation rate, possibly within single magneto-chrons. These results can be used to determine which GPTS provides the best depiction of the depositional history at Smirra. The (e-)ASM-derived sedimentation rates within Chron C24n vary between  $\sim 0.67$  cm/kyr and  $0.82$  cm/kyr (on average) and generally fall in between sedimentation rate values derived from GPTS2004 and CK95 (see Fig. 5). On the other hand, the stable accumulation rate of  $0.65$  cm/kyr in Chron C23r is in good agreement with GPTS2012 (Fig. 8E), while the values for C23n.2n to C22r ( $\sim 0.63$  to  $\sim 0.64$  cm/kyr) and C22n to C21r ( $\sim 1.07$  to  $\sim 1.14$  cm/kyr) are all in good agreement with CK95. The estimates for C22n and C21r, however, would decrease by  $\sim 5\%$ , if data points around  $\sim 0.7$  cm/kyr (at  $\sim 20$  mcd and  $29$  mcd) were included in computing the average sedimentation rates; this would be in better agreement with GTS2012 (Fig. 8E).

The estimated sedimentation rates determined through (e-)ASM analysis can also be used to calculate the duration of Chrons C24n.3n to C21r (Fig. 8F, Table S6). Our data are in general good agreement with the Chron durations inferred from the different GPTSs as well as from recent astrochronologic age models (Galeotti et al., 2017; Westerhold et al., 2017).

However, our analysis also shows possible implications for improving the accuracy of the geologic time scale (GTS). In fact, the main discrepancy between the astronomical and radioisotopic ages in the most recent GTS2012 (see Vandenbergh et al., 2012 and reference therein) stems from a shorter duration of Chron C23n, causing a  $\sim 500$  kyr duration offset up to C21n. Inferred sedimentation rates for C23n.2n and C22r lead to a duration for these (sub)chrons of  $\sim 720$  kyr and  $\sim 950$  kyr (Fig. 8F), respectively, i.e. in relatively good agreement with durations based on CK95 (696 and 1064 kyr) and the radioisotopic age model in GTS2012 (870 and 1280 kyr). However, a possible bias

induced by an undetected faulting within C22r must be taken into account, as this would affect the correct identification of the orbital signal in the lithology leading to an underestimation of either the sedimentation rate or the associated chron duration.

The sedimentation rate estimates for Chron C23n are in agreement with the “3-cycle option” recently proposed by Lauretano et al. (2016) for ODP Site 1263 (see also Galeotti et al., 2017 and Westerhold et al., 2017), rather than with the 2-cycle age model proposed for the same site, which is consistent with the initial astronomically tuned age model of Westerhold and Röhl (2009) for ODP Site 1258. The estimated duration for Chron C23n.2n of  $\sim 720$  kyr in fact, makes it possible to accommodate an extra  $\sim 405$ -kyr cycle within C23n and therefore helps solving this critical time scale issue.

In this view, our results from the Smirra cores show high potential for disentangling the differences observed around 50 Ma between the astronomical and the radio-isotopic age models in GTS2012 (Vandenbergh et al., 2012), being an important step forward in closing the Eocene gap in the astronomical time scale. A robust age model through detailed cyclostratigraphic analysis and astronomical tuning of multi-proxy records of the Smirra cores, preferably validated through detailed analysis of spreading rates among different oceanic basins (e.g. Bouligand et al., 2006), is needed to corroborate the evidence presented here by (e-)ASM analysis of the MS record.

## 6. Conclusions

We provided a new magneto-biostratigraphic record from a  $\sim 93$  m core drilled at Smirra where a continuous and expanded lower Paleogene sedimentary record was recovered.

The Smirra cores span the interval from  $\sim 47$  to  $\sim 60$  Ma, i.e. from the late Paleocene into the middle Eocene. This interpretation is corroborated by a detailed calcareous nannofossil biostratigraphy comprising eleven biozones from CNP11 to CNE10. The detailed magnetostratigraphy has been correlated to available GPTSs and reference sections, confirming the reliability of our magnetic polarity interpretation and showing that the Smirra cores represent one of the most complete records available worldwide.

Sedimentation rates at Smirra highlight remarkable differences between different GPTSs, especially for subchrons within C23n and C24n. These discrepancies could be attributed to discontinuities in the sedimentary record as well as to imprecise dating of (sub)chrons in the reference time scales. Cyclostratigraphic interpretation of the magnetic susceptibility record of the Smirra cores in combination with statistical analysis (i.e. (e-)ASM) of this high-resolution record can be used to obtain an independent assessment of sedimentation rates and constrain the depositional history of the Smirra cores in detail. This analysis provides helpful insights to tackle existing uncertainties in the Paleogene Time Scale, especially concerning the so-called 50 Ma discrepancy in GTS2012. The magnetochron durations derived by the (e-)ASM analysis are, in fact, in close agreement with recent astrochronologic age models and point to a duration of about three 405-kyr eccentricity-related cycles of Chron C23n. This outcome requires further cyclostratigraphic analysis of additional proxy records of the Smirra cores. At present, the age-calibrated magneto- bio- stratigraphy documented in the Smirra succession represents a solid integrated stratigraphic framework to be used as reference for future studies on the late Paleocene to middle Eocene as well as a basis for further improvements of the geologic time scale.

## Acknowledgments

We thank Editor Thomas Algeo and two anonymous reviewers for valuable comments that greatly improved the manuscript. This research was funded by NWO-ALW VICI grant [project number 865.10.001] to L.J. Lourens and supported by funds provided by MIUR-PRIN [grant number 2010X3PP8J\_005] to S. Galeotti. We thank Mr. Marucchini for

allowing access and permits to drill in the Smirra quarry, and Fabio Baio and Geoprove di Kistic Andrea & C. s.n.c. for the technical support during the drilling. We are grateful to the Royal Netherlands Institute for Sea Research (NIOZ) and Rineke Gieles for technical help and analytical support.

## Appendix A. Supplementary data

Supplementary data to this article can be found online at <http://dx.doi.org/10.1016/j.palaeo.2017.08.031>.

## References

- Agnini, C., Muttoni, G., Kent, D.V., Rio, D., 2006. Eocene biostratigraphy and magnetic stratigraphy from Possagno, Italy: the calcareous nannofossil response to climate variability. *Earth Planet. Sci. Lett.* 241, 815–830. <http://dx.doi.org/10.1016/j.epsl.2005.11.005>.
- Agnini, C., Fornaciari, E., Raffi, I., Rio, D., Röhl, U., Westerhold, T., 2007. High-resolution nannofossil biochronology of middle Paleocene to early Eocene at ODP Site 1262: implications for calcareous nannoplankton evolution. *Mar. Micropaleontol.* 64, 215–248. <http://dx.doi.org/10.1016/j.marmicro.2007.05.003>.
- Agnini, C., Fornaciari, E., Giusberti, L., Grandesso, P., Lanci, L., Luciani, V., Muttoni, G., Pali, H., Rio, D., Spofforth, D.J.A., Stefani, C., 2011. Integrated biomagnetostratigraphy of the Alano section (NE Italy): a proposal for defining the middle-late Eocene boundary. *Geol. Soc. Am. Bull.* 123, 841–872. <http://dx.doi.org/10.1130/B30158.1>.
- Agnini, C., Fornaciari, E., Raffi, I., Catanzariti, R., Heiko, P., Backman, J., Rio, D., 2014. Biozonation and biochronology of Paleogene calcareous nannofossils from low and middle latitudes. *News. Stratigr.* 47, 131–181.
- Alvarez, W., Montanari, A., 1988. The Scaglia Limestones (Late Cretaceous–Oligocene) in the northeastern Apennines carbonate sequence: stratigraphic context and geological significance. In: Premoli Silva, I., Coccioni, R., Montanari, A. (Eds.), *The Eocene–Oligocene boundary in the Marche–Umbria Basin (Italy)*. *Int. Subcomm. Paleog. Strat., E-O Meeting, Ancona, Oct. 1987*. Industrie Grafiche Aniballi, Ancona, pp. 13–29.
- Arthur, M.A., Fischer, A., 1977. Upper Cretaceous–Paleocene magnetic stratigraphy at Gubbio, Italy. I. Lithostratigraphy and sedimentology. *Geol. Soc. Am. Bull.* 88 (3), 367–371. [http://dx.doi.org/10.1130/0016-7606\(1977\)88<367:UCMSAG>2.0.CO;2](http://dx.doi.org/10.1130/0016-7606(1977)88<367:UCMSAG>2.0.CO;2).
- Backman, J., 1986. Late Paleocene to middle Eocene calcareous nannofossil biochronology from the Shatsky Rise, Walvis Ridge and Italy. *Palaeogeogr. Palaeoclimatol. Palaeoecol.* 57, 43–59.
- Besse, J., Courtillot, V., 2002. Apparent and true polar wander and the geometry of the geomagnetic field over the last 200 Myr. *J. Geophys. Res.* 107, 2300–2331. <http://dx.doi.org/10.1029/2000JB000050>.
- Bouligand, C., Dymant, J., Gallet, Y., Hulot, G., 2006. Geomagnetic field variations between chronos 33r and 19r (83–41 Ma) from sea-surface magnetic anomaly profiles. *Earth Planet. Sci. Lett.* 250, 541–560. <http://dx.doi.org/10.1016/j.epsl.2006.06.051>.
- Bowles, J., 2006. Data report: revised magnetostratigraphy and magnetic mineralogy of sediments from Walvis Ridge, Leg 208. In: Kroon, D., Zachos, J.C., Richter, C. (Eds.), *Proc. ODP, Sci. Results. Vol. 208*. Ocean Drilling Program, College Station, TX, pp. 1–24.
- Bown, P.R., Young, J.R., 1998. Techniques. In: Bown, P.R. (Ed.), *British Micropaleontological Society Publication Series*. Kluwer Academic Publishers, Cambridge V. of 315 pp.
- Butler, R.F., Gingerich, P.D., Lindsay, E.H., 1981. Magnetic polarity stratigraphy and biostratigraphy of Paleocene and lower Eocene continental deposits, Clarks Fork Basin, Wyoming. *J. Geol.* 89, 299–316.
- Cande, S.C., Kent, D.V., 1992. A new geomagnetic polarity time scale for the Late Cretaceous and Cenozoic. *J. Geophys. Res.* 97, 13917–13951.
- Cande, S.C., Kent, D.V., 1995. Revised calibration of the geomagnetic polarity time scale for the Late Cretaceous and Cenozoic. *J. Geophys. Res.* 100 (B4), 6093–6096. <http://dx.doi.org/10.1029/94JB03098>.
- Channell, J.E.T., d'Argenio, B., Horvath, F., 1979. Adria, the African promontory, in Mesozoic Mediterranean palaeogeography. *Earth Sci. Rev.* 15 (3), 213–292. [http://dx.doi.org/10.1016/0012-8252\(79\)90083-7](http://dx.doi.org/10.1016/0012-8252(79)90083-7).
- Channell, J.E.T., Freeman, R., Heller, F., Lowrie, W., 1982. Timing of diagenetic haematite growth in red pelagic limestones from Gubbio (Italy). *Earth Planet. Sci. Lett.* 58, 189–201. [http://dx.doi.org/10.1016/0012-821X\(82\)90193-5](http://dx.doi.org/10.1016/0012-821X(82)90193-5).
- Ciarapica, G., Passeri, L., 2002. The palaeogeographic duplicity of the Apennines. *Boll. Soc. Geol. Ital.* 121 (1), 67–75.
- Clyde, W.C., 2001. Mammalian biostratigraphy of the McCullough Peaks area in the northern Bighorn Basin, Bighorn Basin magnetostratigraphy. In: Gingerich, P.D. (Ed.), *Paleocene–Eocene Stratigraphy and Biotic Change in the Bighorn and Clarks Fork Basins*. 33. University of Michigan Papers on Paleontology, Wyoming, pp. 109–126.
- Clyde, W.C., Stamatakis, J., Gingerich, P.D., 1994. Chronology of the Wasatchian land-mammal age (early Eocene): magnetostratigraphic results from the McCullough Peaks section, northern Bighorn Basin, Wyoming. *J. Geol.* 102, 367–377.
- Coccioni, R., Frontalini, F., Bancalà, G., Fornaciari, E., Jovane, L., Sprovieri, M., 2010. The Dan-C2 hyperthermal event at Gubbio (Italy): global implications, environmental effects, and cause(s). *Earth Planet. Sci. Lett.* 297, 298–305. <http://dx.doi.org/10.1016/j.epsl.2010.06.031>.
- Coccioni, R., Bancalà, G., Catanzariti, R., Fornaciari, E., Frontalini, F., Giusberti, L., Jovane, L., Luciani, V., Savian, J., Sprovieri, M., 2012. An integrated stratigraphic record of the Paleocene–lower Eocene at Gubbio (Italy): new insights into the early Paleogene hyperthermals and carbon isotope excursions. *Terra Nova* 24, 380–386. <http://dx.doi.org/10.1111/j.1365-3121.2012.01076.x>.
- Coccioni, R., Sideri, M., Bancalà, G., Catanzariti, R., Frontalini, F., Jovane, L., Montanari, A., Savian, J.F., 2013. Integrated stratigraphy (magneto-, bio- and chronostratigraphy) and geochronology of the Paleogene pelagic succession of the Umbria–Marche Basin (central Italy). *Geol. Soc. Lond., Spec. Publ.* 373 (1), 111–131. <http://dx.doi.org/10.1144/SP373.4>.
- Coccioni, R., Catanzariti, R., Frontalini, F., Galbrun, B., Jovane, L., Montanari, A., Savian, J.F., Sideri, M., 2016. Integrated magnetostratigraphy, biostratigraphy, and chronostratigraphy of the Paleogene pelagic succession at Gubbio (central Italy). In: Menichetti, M., Coccioni, R., Montanari, A. (Eds.), *The Stratigraphic Record of Gubbio: Integrated Stratigraphy of the Late Cretaceous–Paleogene Umbria–Marche Pelagic Basin*. 524. Geological Society of America Special Paper, pp. 139–160. [http://dx.doi.org/10.1130/2016.2524\(10\)](http://dx.doi.org/10.1130/2016.2524(10)).
- Cogné, J.P., 2003. PaleoMac: a Macintosh™ application for treating paleomagnetic data and making plate reconstructions. *Geochim. Geophys. Geosyst.* 4 (1). <http://dx.doi.org/10.1029/2001GC000227>.
- Dallanave, E., Agnini, C., Muttoni, G., Rio, D., 2009. Magneto-biostratigraphy of the Cicogna section (Italy): implications for the late Paleocene–early Eocene time scale. *Earth Planet. Sci. Lett.* 285, 39–51. <http://dx.doi.org/10.1016/j.epsl.2009.05.033>.
- Dallanave, E., Agnini, C., Muttoni, G., Rio, D., 2012. Paleocene magneto-biostratigraphy and climate-controlled rock magnetism from the Belluno Basin, Tethys Ocean, Italy. *Palaeogeogr. Palaeoclimatol. Palaeoecol.* 337–338, 130–142. <http://dx.doi.org/10.1016/j.palaeo.2012.04.007>.
- Dallanave, E., Agnini, C., Bachtadse, V., Muttoni, G., Crampton, J.S., Strong, C.P., Hines, B.R., Hollis, C.J., Slotnick, B.S., 2015. Early to middle Eocene magneto-biochronology of the southwest Pacific Ocean and climate influence on sedimentation: insights from the Mead Stream section, New Zealand. *Geol. Soc. Am. Bull.* 127, 643–660. <http://dx.doi.org/10.1130/B31147.1>.
- Dallanave, E., Bachtadse, V., Crouch, E.M., Tauxe, L., Shepherd, C.L., Morgans, H.E.G., Hollis, C.J., Hines, B.R., Sugisaki, S., 2016. Constraining early to middle Eocene climate evolution of the southwest Pacific and Southern Ocean. *Earth Planet. Sci. Lett.* 433, 380–392. <http://dx.doi.org/10.1016/j.epsl.2015.11.010>.
- D'Argenio, B., 1970. Evoluzione geotettonica comparata tra alcune piattaforme carbonatiche dei Mediterraneo Europeo ed Americano. *Atti Accademia Pontiana* 20, 3–34.
- Dekkers, M.J., Linssen, J.H., 1989. Rockmagnetic properties of fine-grained natural low-temperature haematite with reference to remanence acquisition mechanisms in red beds. *Geophys. J. Int.* 99 (1), 1–18. <http://dx.doi.org/10.1111/j.1365-246X.1989.tb02012.x>.
- Dinarès-Turell, J., Baceta, J.I., Pujalte, V., Orue-Etxebarria, X., Bernaola, G., 2002. Magnetostratigraphic and cyclostratigraphic calibration of a prospective Paleocene/Eocene stratotype at Zumaia (Basque Basin, Northern Spain). *Terra Nova* 14 (5), 371–378. <http://dx.doi.org/10.1046/j.1365-3121.2002.00431.x>.
- Dinarès-Turell, J., Baceta, J.I., Pujalte, V., Orue-Etxebarria, X., Bernaola, G., Lorito, S., 2003. Untangling the Paleocene climatic rhythm: an astronomically calibrated Early Paleocene magnetostratigraphy and biostratigraphy at Zumaia (Basque Basin, Northern Spain). *Earth Planet. Sci. Lett.* 216, 483–500. [http://dx.doi.org/10.1016/S0012-821X\(03\)00557-0](http://dx.doi.org/10.1016/S0012-821X(03)00557-0).
- Dinarès-Turell, J., Baceta, J.I., Bernaola, G., Orue-Etxebarria, X., Pujalte, V., 2007. Closing the Mid-Paleocene gap: toward a complete astronomically tuned Paleocene Epoch and Selandian and Thanetian GSSPs at Zumaia (Basque Basin, W Pyrenees). *Earth Planet. Sci. Lett.* 262, 450–467.
- Edgar, K.M., Wilson, P.A., Sexton, P.F., Gibbs, S.J., Roberts, A.P., Norris, R.D., 2010. New biostratigraphic, magnetostratigraphic and isotopic insights into the middle Eocene climatic optimum in low latitudes. *Palaeogeogr. Palaeoclimatol. Palaeoecol.* 297, 670–682. <http://dx.doi.org/10.1016/j.palaeo.2010.09.016>.
- Ellwood, B.B., Crick, R.E., El Hassani, A., Benoist, S.L., Young, R.H., 2000. Magneto-susceptibility event and cyclostratigraphy method applied to marine rocks: detrital input versus carbonate productivity. *Geology* 28 (12), 1135–1138. [http://dx.doi.org/10.1130/0091-7613\(2000\)28<1135:MEACMA>2.0.CO;2](http://dx.doi.org/10.1130/0091-7613(2000)28<1135:MEACMA>2.0.CO;2).
- Florindo, F., Roberts, A.P., 2005. Eocene–Oligocene magnetobiochronology of ODP Sites 689 and 690, Maud Rise, Weddell Sea, Antarctica. *Geol. Soc. Am. Bull.* 117, 46–66. <http://dx.doi.org/10.1130/B25541.1>.
- Franceschi, M., Penasa, L., Coccioni, R., Gattacceca, J., Smit, J., Cascella, A., Mariani, S., Montanari, A., 2015. Terrestrial Laser Scanner imaging for the cyclostratigraphy and astronomical tuning of the Ypresian–Lutetian pelagic section of Smirra (Umbria–Marche Basin, Italy). *Palaeogeogr. Palaeoclimatol. Palaeoecol.* 440, 33–46. <http://dx.doi.org/10.1016/j.palaeo.2015.08.027>.
- Galeotti, S., Angori, E., Coccioni, R., Ferrari, G., Galbrun, B., Monechi, S., Premoli Silva, I., Speijer, R., Turi, B., 2000. Integrated stratigraphy across the Paleocene/Eocene boundary in the Contessa Road section, Gubbio (central Italy). *Bulletin de la Société Géologique de France* 171, 355–365.
- Galeotti, S., Kaminski, M.A., Speijer, R., Coccioni, R., 2004. High resolution Deep Water Agglutinated Foraminiferal record across the Paleocene/Eocene transition in the Contessa Road section (central Italy). In: Bubik, M., Kaminski, M.A. (Eds.), *Proceedings of the 6th International Workshop on Agglutinated Foraminifera*. Arti Grafiche Editoriali. 8. Grzybowski Foundation Special Publication, Urbino, pp. 83–103.
- Galeotti, S., Krishnan, S., Pagani, M., Lanci, L., Gaudio, A., Zachos, J.C., Monechi, S., Morelli, G., Lourens, L., 2010. Orbital chronology of Early Eocene hyperthermals from the Contessa Road section, central Italy. *Earth Planet. Sci. Lett.* 290, 192–200. <http://dx.doi.org/10.1016/j.epsl.2009.12.021>.
- Galeotti, S., Moretti, M., Cappelli, C., Phillips, J., Lanci, L., Littler, K., Monechi, S.,

- Petrizzo, M.R., Silva, I.P., Zachos, J.C., 2015. The Bottaccione section at Gubbio, central Italy: a classical Paleocene Tethyan setting revisited. *Newsl. Stratigr.* 48, 325–339. <http://dx.doi.org/10.1127/nos/2015/0067>.
- Galeotti, S., Moretti, M., Sabatino, N., Sprovieri, M., Ceccatelli, M., Francescone, F., Lauretano, V., Monechi, S., 2017. Cyclochronology of the Early Eocene carbon isotope record from a composite succession of the classic Contessa and Bottaccione sections (Gubbio, central Italy). *Newsl. Stratigr.* 50 (3), 231–244.
- Giuseberti, L., Coccioni, R., Sprovieri, M., Tateo, F., 2009. Perturbation at the sea floor during the Paleocene-Eocene Thermal Maximum: evidence from benthic foraminifera at Contessa Road, Italy. *Mar. Micropaleontol.* 70, 102–119. <http://dx.doi.org/10.1016/j.marmicro.2008.11.003>.
- Gradstein, F.M., Ogg, J.G., Smith, A.G., 2004. *A Geologic Time Scale*. Cambridge University Press, Cambridge, UK (589 pp).
- Gradstein, F.M., Ogg, J.G., Schmitz, M.D., Ogg, G.M., 2012. *The Geologic Time Scale*. Elsevier, Amsterdam, The Netherlands (1176 pp).
- Jovane, L., Florindo, F., Coccioni, R., Dinarès-Turell, J., Marsili, A., Monechi, S., Roberts, A.P., Sprovieri, M., 2007. The middle Eocene climatic optimum event in the Contessa Highway section, Umbrian Apennines, Italy. *Geol. Soc. Am. Bull.* 119, 413–427. <http://dx.doi.org/10.1130/B25917.1>.
- Kirschvink, J.L., 1980. The least-squares line and plane and analysis of paleomagnetic data. *Geophys. J. R. Astron. Soc.* 62 (3), 699–718. <http://dx.doi.org/10.1111/j.1365-246X.1980.tb02601.x>.
- Kirtland Turner, S., Sexton, P.F., Charles, C.D., Norris, R.D., 2014. Persistence of carbon release events through the peak of early Eocene global warmth. *Nat. Geosci.* 7, 748–751. <http://dx.doi.org/10.1038/ngeo2240>.
- Lanci, L., Lowrie, W., Montanari, A., 1996. Magnetostratigraphy of the Eocene-Oligocene boundary in a short drill-core. *Earth Planet. Sci. Lett.* 143, 37–48. [http://dx.doi.org/10.1016/0012-821X\(96\)00136-7](http://dx.doi.org/10.1016/0012-821X(96)00136-7).
- Laskar, J., Robutel, P., Joutel, F., Gastineau, M., Correia, A.C.M., Levrard, B., 2004. A long-term numerical solution for the insolation quantities of the Earth. *Astron. Astrophys.* 428, 261–285. <http://dx.doi.org/10.1051/0004-6361:20041335>.
- Lauretano, V., Littler, K., Polling, M., Zachos, J.C., Lourens, L.J., 2015. Frequency, magnitude and character of hyperthermal events at the onset of the Early Eocene Climatic Optimum. *Clim. Past* 11, 1313–1324. <http://dx.doi.org/10.5194/cp-11-1313-2015>.
- Lauretano, V., Hilgen, F.J., Zachos, J.C., Lourens, L.J., 2016. Astronomically tuned age model for the early Eocene carbon isotope events: a new high-resolution  $\delta^{13}\text{C}_{\text{benthic}}$  record of ODP Site 1263 between ~49 and ~54 Ma. *Newsl. Stratigr.* <http://dx.doi.org/10.1127/nos/2016/0077>.
- Littler, K., Röhl, U., Westerhold, T., Zachos, J.C., 2014. A high-resolution benthic stable-isotope record for the South Atlantic: implications for orbital-scale changes in Late Paleocene–Early Eocene climate and carbon cycling. *Earth Planet. Sci. Lett.* 401, 18–30. <http://dx.doi.org/10.1016/j.epsl.2014.05.054>.
- Lourens, L.J., Sluijs, A., Kroon, D., Zachos, J.C., Thomas, E., Röhl, U., Bowles, J., Raffi, I., 2005. Astronomical pacing of late Palaeocene to early Eocene global warming events. *Nature* 435, 1083–1087. <http://dx.doi.org/10.1038/nature03814>.
- Lowrie, W., 1990. Identification of ferromagnetic minerals in a rock by coercivity and unblocking temperature properties. *Geophys. Res. Lett.* 17 (2), 159–162.
- Lowrie, W., Alvarez, W., 1977. Upper Cretaceous–Paleocene magnetic stratigraphy at Gubbio, Italy: III. Magnetic stratigraphy. *Geol. Soc. Am. Bull.* 88, 374–377. [http://dx.doi.org/10.1130/0016-7606\(1977\)88<374:UCMSAG>2.0.CO;2](http://dx.doi.org/10.1130/0016-7606(1977)88<374:UCMSAG>2.0.CO;2).
- Lowrie, W., Channell, J.E.T., Alvarez, W., 1980. A review of magnetic stratigraphy investigations in Cretaceous pelagic carbonate rocks. *J. Geophys. Res.* 85 (B7), 3597–3605. <http://dx.doi.org/10.1029/JB085iB07p03597>.
- Lowrie, W., Napoleone, G., Perch-Nielsen, K., Premoli Silva, I., Toumarkine, M., 1982. Paleogene magnetic stratigraphy in Umbrian pelagic carbonate rocks: the Contessa sections, Gubbio. *Geol. Soc. Am. Bull.* 93, 414–432. [http://dx.doi.org/10.1130/0016-7606\(1982\)93<414:PMSIUP>2.0.CO;2](http://dx.doi.org/10.1130/0016-7606(1982)93<414:PMSIUP>2.0.CO;2).
- Ma, C., Meyers, S.R., Sageman, B.B., Singer, B.S., Jicha, B.R., 2014. Testing the astronomical time scale for oceanic anoxic event 2, and its extension into Cenomanian strata of the Western Interior Basin (USA). *Geol. Soc. Am. Bull.* 126, 974–989. <http://dx.doi.org/10.1130/B30922.1>.
- Martini, E., 1971. Standard Tertiary and Quaternary calcareous nannoplankton zonation. In: Farinacci, A. (Ed.), *Proceedings of the Second Planktonic Conference*, Roma 1970, pp. 739–785 (Tecnoscienza).
- McFadden, P.L., Reid, B., 1982. Analysis of palaeomagnetic inclination data. *Geophys. J. R. Astron. Soc.* 69, 307–319.
- Meyers, S.R., Hinnov, L.A., 2010. Northern Hemisphere glaciation and the evolution of Plio-Pleistocene climate noise. *Paleoceanography* 25, PA3207. <http://dx.doi.org/10.1029/2009PA001834>.
- Meyers, S.R., Sageman, B.B., 2007. Quantification of deep-time orbital forcing by average spectral misfit. *Am. J. Sci.* 307, 773–792. <http://dx.doi.org/10.2475/05.2007.01>.
- Meyers, S.R., Sageman, B., Hinnov, L., 2001. Integrated quantitative stratigraphy of the Cenomanian-Turonian Bridge Creek Limestone Member using evolutive harmonic analysis and stratigraphic modeling. *J. Sediment. Res.* 71 (4), 628–644. <http://dx.doi.org/10.1306/012401710628>.
- Meyers, S.R., Sageman, B.B., Arthur, M.A., 2012. Obliquity forcing of organic matter accumulation during Oceanic Anoxic Event 2. *Paleoceanography* 27, PA3212. <http://dx.doi.org/10.1029/2012PA002286>.
- Monechi, S., Thierstein, H., 1985. Late Cretaceous–Eocene nanofossil and magnetotratigraphic correlations near Gubbio, Italy. *Mar. Micropaleontol.* 9, 419–440. [http://dx.doi.org/10.1016/0377-8398\(85\)90009-X](http://dx.doi.org/10.1016/0377-8398(85)90009-X).
- Muttoni, G., Kent, D.V., 2007. Widespread formation of cherts during the early Eocene climatic optimum. *Palaeogeogr. Palaeoclimatol. Palaeoecol.* 253 (3), 348–362.
- Napoleone, G., Premoli Silva, I., Heller, F., Cheli, P., Corezzi, S., Fischer, A.G., 1983. Eocene magnetic stratigraphy at Gubbio, Italy, and its implications for Paleogene geochronology. *Geol. Soc. Am. Bull.* 94 (2), 181–191. [http://dx.doi.org/10.1130/0016-7606\(1983\)94<181:EMSAGI>2.0.CO;2](http://dx.doi.org/10.1130/0016-7606(1983)94<181:EMSAGI>2.0.CO;2).
- Nicolo, M.J., Dickens, G.R., Hollis, C.J., Zachos, J.C., 2007. Multiple early Eocene hyperthermals: their sedimentary expression on the New Zealand continental margin and in the deep sea. *Geology* 35, 699–702. <http://dx.doi.org/10.1130/G23648A.1>.
- Ogg, J., Bardot, L., 2001. Aptian through Eocene magnetostratigraphic correlation of the Blake Nose transect (Leg 171B), Florida continental margin. In: Kroon, D., Norris, R.D., Klaus, A. (Eds.), *Proceedings of the Ocean Drilling Program, Scientific Results. Volume 171B. Ocean Drilling Program, College Station, Texas*, pp. 1–58.
- Okada, H., Bukry, D., 1980. Supplementary modification and introduction of code numbers to the low latitude coccolith biostratigraphic zonation (Bukry, 1973; 1975). *Mar. Micropaleontol.* 5, 321–325. [http://dx.doi.org/10.1016/0377-8398\(80\)90016-X](http://dx.doi.org/10.1016/0377-8398(80)90016-X).
- Parès, J.M., Lanci, L., 2004. A middle Eocene–early Miocene magnetic polarity stratigraphy in equatorial Pacific sediments (ODP Site 1220). In: Channell, J.E.T., Kent, D.V., Lowrie, W., Meert, J.G. (Eds.), *Timescales of the Paleomagnetic Field: American Geophysical Union Geophysical Monograph*. 145, pp. 131–140.
- Reynolds, R.L., King, J.W., 1995. Magnetic records of climate-change. *Rev. Geophys.* 33 (S1), 101–110. <http://dx.doi.org/10.1029/95RG00354>.
- Satolli, S., Turtù, A., 2016. Early Cretaceous magnetostratigraphy of the Salto del Cieco section (Northern Apennines, Italy). *Newsl. Stratigr.* <http://dx.doi.org/10.1127/nos/2016/0076>.
- Satolli, S., Besse, J., Calamita, F., 2008. Paleomagnetism of Aptian–Albian sections from the Northern Apennines (Italy): implications for the 150–100 Ma apparent polar wander of Adria and Africa. *Earth Planet. Sci. Lett.* 276 (1), 115–128.
- Satolli, S., Turtù, A., Donatelli, U., 2015. Magnetostratigraphy of the Salto del Cieco section (Northern Apennines, Italy) from the Pliensbachian to Jurassic/Cretaceous boundary. *Newsl. Stratigr.* 48, 153–177. <http://dx.doi.org/10.1127/nos/2015/0058>.
- Speranza, F., Satolli, S., Mattioli, E., Calamita, F., 2005. Magnetic stratigraphy of Kimmeridgian–Aptian sections from Umbria–Marche (Italy): new details on the M polarity sequence. *J. Geophys. Res. Solid Earth* 110, B12109. <http://dx.doi.org/10.1029/2005JB003884>.
- Suganuma, Y., Ogg, J., 2006. Campanian through Eocene magnetostratigraphy of Sites 1257–1261, ODP Leg 207, Demerara Rise (western Equatorial Atlantic). In: Mosher, D.C., Erbacher, J., Malone, M.J. (Eds.), *Proceeding of the Ocean Drilling Program, Scientific Results. 207. Ocean Drilling Program, College Station, Texas*, pp. 1–48.
- Tauxe, L., Kent, D.V., Opdyke, N.D., 1980. Magnetic components contributing to the NRM of Middle Siwalik red beds. *Earth Planet. Sci. Lett.* 47 (2), 279–284.
- Torrence, C., Compo, G.P., 1998. A practical guide to wavelet analysis. *Bull. Am. Meteorol. Soc.* 79, 61–78. [http://dx.doi.org/10.1175/1520-0477\(1998\)079<0061:APGTWA>2.0.CO;2](http://dx.doi.org/10.1175/1520-0477(1998)079<0061:APGTWA>2.0.CO;2).
- Turtù, A., Satolli, S., Maniscalco, R., Calamita, F., Speranza, F., 2013. Understanding progressive-arc- and strike-slip-related rotations in curve-shaped orogenic belts: the case of the Olevano-Anrodoco-Sibillini thrust (Northern Apennines, Italy). *J. Geophys. Res. Solid Earth* 118, 459–473. <http://dx.doi.org/10.1002/jgrb.50096>.
- Vandenbergh, N., Hilgen, F.J., Speijer, R.P., Ogg, J.G., Gradstein, F.M., Hammer, O., Hollis, C.J., Hooker, J.J., 2012. The Paleogene Period. In: *The Geologic Time Scale 2012*. Elsevier, Boston, pp. 855–921. <http://dx.doi.org/10.1016/B978-0-444-59425-9.00028-7>.
- Westerhold, T., Röhl, U., 2009. High resolution cyclostratigraphy of the early Eocene–new insights into the origin of the Cenozoic cooling trend. *Clim. Past* 5 (3), 309–327.
- Westerhold, T., Röhl, U., Raffi, I., Fornaciari, E., Monechi, S., Reale, V., Bowles, J., Evans, H.F., 2008. Astronomical calibration of the Paleocene time. *Palaeogeogr. Palaeoclimatol. Palaeoecol.* 257, 377–403. <http://dx.doi.org/10.1016/j.palaeo.2007.09.016>.
- Westerhold, T., Röhl, U., Frederichs, T., Bohaty, S.M., Zachos, J.C., 2015. Astronomical calibration of the geological timescale: closing the middle Eocene gap. *Clim. Past* 11, 1181–1195. <http://dx.doi.org/10.5194/cp-11-1181-2015>.
- Westerhold, T., Röhl, U., Frederichs, T., Agnini, C., Raffi, I., Zachos, J.C., Wilkens, R.H., 2017. Astronomical calibration of the Ypresian time scale: implications for seafloor spreading rates and the chaotic behaviour of the solar system? *Clim. Past Discuss.* <http://dx.doi.org/10.5194/cp-2017-15>. (in review).
- Zachos, J.C., Röhl, U., Schellenberg, S.A., Sluijs, A., Hodell, D.A., Kelly, D.C., Thomas, E., Nicolo, M., Raffi, I., Lourens, L.J., McCarren, H., Kroon, D., 2005. Rapid acidification of the ocean during the paleocene–eocene thermal maximum. *Science* 308, 1611–1615. <http://dx.doi.org/10.1126/science.1109004>.
- Zachos, J.C., Dickens, G.R., Zeebe, R.E., 2008. An early Cenozoic perspective on greenhouse warming and carbon-cycle dynamics. *Nature* 451, 279–283. <http://dx.doi.org/10.1038/nature06588>.
- Zijderveld, J.D.A., 1967. A.C. demagnetization of rocks: analysis of results. In: Collinson, D.W. (Ed.), *Methods in Paleomagnetism*. Elsevier, Amsterdam, pp. 254–286.